Chapter 6

The Hodgkin and Huxley Model of Action Potential Generation

The vast majority of nerve cells generate a series of brief voltage pulses in response to vigorous input. These pulses, also referred to as *action potentials* or *spikes*, originate at or close to the cell body, and propagate down the axon at constant velocity and amplitude. The composite figure 6.1 shows the shape of the action potential from a number of different neuronal and non-neuronal preparations. Action potentials come in a variety of shapes; common to all is the all-or-none depolarization of the membrane beyond 0 mV. That is, if the voltage fails to exceed a particular threshold value, no spike is initiated and the potential returns to its baseline level. If the voltage threshold is exceeded, the membrane executes a stereotyped voltage trajectory that reflects membrane properties and not the input. As evident in Fig. 6.1, the shape of the action potential can vary enormously from cell type to cell type.

When inserting an electrode into a brain, the small all-or-none electrical events one observes extracellularly are usually due to spikes that are initiated close to the cell body and that propagate along the axons. These spikes have but a single peak between +10 and +30 mV and are over (depending on the temperature) within one or two milliseconds. Other all-or-none events, such as the complex spikes in cerebellar Purkinje cells (Fig. 6.1G) or bursting pyramidal cells in cortex (Fig. 6.1H and Fig. 16.1) show a more complex wave form with one or more fast spikes superimposed onto an underlying, much slower depolarization. Finally, under certain conditions, the dendritic membrane can also generate all-or-none events (Fig. 6.1H) that are much slower than somatic spikes, usually on the order to 50-100 msec or longer. We will treat these events and their possible significance in chapter 19.

Only a small fraction of all neurons are unable—under physiological conditions—to generate action potentials, making exclusive use of graded signals. Examples of such *non-spiking cells*, usually spatially compact, can be found in the distal retina (e.g. bipolar, horizontal and certain types of amacrine cells) and many neurons in the sensory-motor pathway of invertebrates (Roberts and Bush, 1981). They appear to be absent from cortex, thalamus, cerebellum and associated structures (although it is difficult, on *a priori* grounds, to com-

pletely rule out their existence).

Action potentials are such a dominant feature of the nervous system that for a considerable amount of time it was widely held—and still is in parts of the theoretical community—that all neuronal computations only involve these all-or-none events. This belief provided much of the impetus behind the neural network models originating in the late 1930s and early 1940s (Rashevsky, 1938; McCullough and Pitts, 1943).

The ionic mechanisms underlying the initiation and propagation of action potentials in nervous tissue were first elucidated in the squid giant axon by a number of workers, most notably by Alan Hodgkin and Andrew Huxley in Cambridge, England (1952a,b,c,d). Together with John Eccles, they shared the 1963 Nobel price in physiology and medicine (for a historical account see Hodgkin, 1976). Their quantitative model (Hodgkin and Huxley, 1952d) represents one of the high points of cellular biophysics and has been extremely influential in terms of enabling a large class of quite diverse membrane phenomena to be analyzed and modeled in terms of simple underlying variables. This is all the more surprising since the kinetic description of membrane permeability changes within the framework of the Hodgkin-Huxely model was achieved without any knowledge of the underlying ionic channels.

A large number of excellent papers and book describing in great detail various aspects of the Hodgkin and Huxley model are available today. Nothing matches the monograph by Jack, Noble and Tsien (1975) for their detailed, 200 page extended coverage of various analytical and numerical approaches to understand all relevant aspects of initiation and conduction of action potentials. Cronin (1987) presents a mathematical account of the more formal aspects of Hodgkin and Huxley's and related model, while Scott (1975) pays particular attention to questions of interest to physicists and applied mathematicians. The books by Hille (1992), Johnston and Wu (1994) and Weiss (1996) provide up-to-date and very readable accounts of the biophysical mechanisms underlying action potential in neuronal tissues. The edited volume by Waxman, Kocsis and Stys (1995) provides more details regarding the morphology and the pathophysiology of myelinated and unmyelinated axons.

Because the biophysical mechanisms underlying action potential generation in the cell body and axons of both invertebrates and vertebrates can be understood and modeled by the formalism Hodgkin and Huxley introduced 40 years ago, it becomes imperative to understand their model and its underlying assumptions. We will strive in this chapter to give an account of those properties of the Hodgkin and Huxley model that are of greatest relevance to understanding the initiation of the action potential. We will also discuss the propagation of spikes along unmyelinated and myelinated fibers. Chapter 9 extends the Hodgkin and Huxley framework to the plethora of other currents described since their days.

6.1 The Basic Assumptions

Hodgkin and Huxley carried out their analysis in the giant axon of the squid. With its half millimeter diameter, this fiber is a leviathan among axons (the typical axon in cortex has a diameter more than one thousand times smaller; Braitenberg and Schüz, 1991). In order to eliminate the complexity introduced by the distributed nature of the cable, a highly conduc-

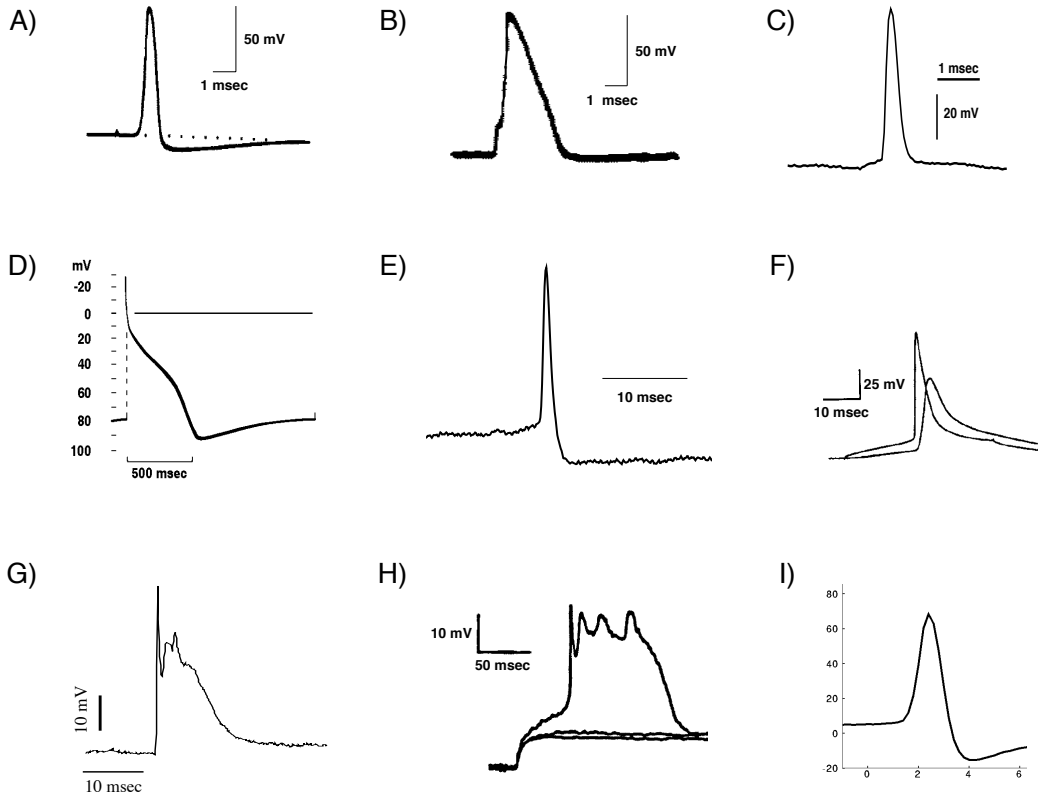

Figure 6.1: Action Potentials of the World

Action potentials in different invertebrate and vertebrate preparations. Common to all is a threshold, below which no impulse is initiated, and a stereotypical shape that depends only on intrinsic membrane properties and not on the type or the duration of the input. **(A)** Giant squid axon at 16° C. From Baker, Hodgkin and Shaw (1962). **(B)** Axonal spike from the node of Ranvier in a myelinated frog fiber at 22° C. From Dodge (1963). **(C)** Cat visual cortex at 37° C. J. Allison, personal communication. **(D)** Sheep heart Purkinje fiber at 10° C. From Weidmann (1956). **(E)** Patch clamp recording from a rabbit retinal ganglion cell at 37° C. F. Amthor, personal communication. **(F)** Layer 5 pyramidal cell in the rat at room temperatures. Simultaneous recordings from the soma and the apical trunk. From Stuart and Sakmann (1994). **(G)** A complex spike—consisting of a large EPSP superimposed onto a slow dendritic calcium spike and several fast somatic sodium spikes—from a Purkinje cell body in the rat cerebellum at 36° C. D. Jaeger, personal communication. **(H)** Layer 5 pyramidal cell in the rat at room temperature. Three dendritic voltage traces in response to three current steps of different amplitude reveal the all-or-none character of this slow event. Notice the fast, superimposed spikes. From Kim and Connors (1993). **(I)** Cell body of a projection neuron in the antennal lobe in the locust at 23° C. G. Laurent, personal communication.

---

tive axial wire was inserted inside the wire. This so called *space clamp* the potential along the entire axon spatially uniform, similar to the situation occurring in a patch of membrane.

This, together with voltage clamping the membrane and the usage of pharmacological agents to block various currents, enabled Hodgkin and Huxley to dissect the membrane current into its constitutive components. The total membrane current is the sum of the ionic currents and the capacitive current:

$$I_m(t) = I_{ionic}(t) + C_m \frac{dV(t)}{dt} . \tag{6.1}$$

With the help of these tools, Hodgkin and Huxley (1952a,b,c) carried out a large number of experiments, which lead them to postulate the following *phenomenological* model of the events underlying the generation of the action potential in the squid giant axon (Fig. 6.2; Hodgkin and Huxley, 1952d)[1].

(i) The action potential involves two major, voltage-dependent ionic conductances, a sodium conductance, G_{Na}, and a potassium conductance, G_K. They are independent from each other. A third, smaller so-called "leak" conductance (which we term G_m), is independent of the membrane potential. The total ionic current flowing is the sum of a sodium, a potassium and the leak current:

$$I_{ionic} = I_{Na} + I_K + I_{leak} . \tag{6.2}$$

(ii) The individual ionic currents $I_i(t)$ are linearly related to the driving potential via Ohm's law:

$$I_i(t) = G_i(V(t), t)(V(t) - E_i) , \tag{6.3}$$

where the ionic reversal potential E_i is given by Nernst's equation for the appropriate ionic species. Depending on the balance between the concentration difference of the ions and the electrical field across the membrane separating the intra- from the extracellular cytoplasm, each ionic species has such as associated *ionic battery* (see eq. 4.3). Conceptually, we can use the equivalent circuit shown in Fig. 6.2 to describe the axonal membrane.

(iii) Each of the two ionic conductances is expressed as a maximum conductance, $\overline{G}_{Na}$ and $\overline{G}_K$, multiplied by a numerical coefficient representing the fraction of the maximum conductance actually open. These numbers are functions of one or more fictive *gating particles* Hodgkin and Huxley introduced to describe the dynamics of the conductances. In their original model, they talked about *activating* and *inactivating* gating particles. Each gating particle can be in one of two possible states, open or close, depending on time and on the membrane potential. In order for the conductance to open, all of these gating particles must be open simultaneously. The entire kinetic properties of their model is contained in these variables. We will consider the physical and molecular interpretation of these gating particles in terms of numerous, all-or-none, microscopic *ionic channels* in the following chapter.

[1]Following our convention, we should express I_m as i_m, since these are currents per unit area. We here follow the established precedent and use capitalized symbols.

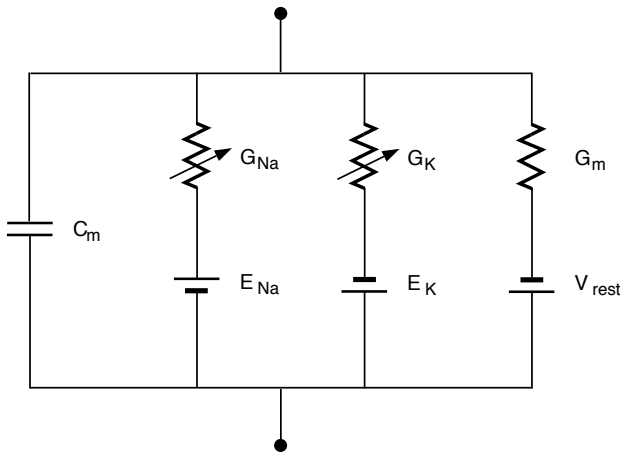

Figure 6.2: ELECTRICAL CIRCUIT FOR A PATCH OF SQUID AXON
Hodgkin and Huxley modeled the membrane of the squid axon using four parallel branches: two passive ones (the membrane capacitance C_m and the leak conductance $G_m = 1/R_m$) and two time- and voltage-dependent ones representing the sodium and the potassium channels.

6.2 Activation and Inactivation States

Let us specify how these activation and inactivation states determine the two ionic currents. This is important, since the vast majority of state-of-the-art ionic models are formulated in terms of such particles.

6.2.1 The Potassium Current I_K

Hodgkin and Huxley (1952d) model the potassium current as

$$I_K = \overline{G}_K n^4 (V - E_K)\,, \tag{6.4}$$

where the maximal conductance $\overline{G}_K = 36\ \mathrm{mS/cm^2}$ and the potassium battery is E_K =-12 mV relative to the resting potential of the axon. n describes the state of a fictional *activation particle*, is a dimensionless number between 0 and 1. Note that with today's physiological conventions, I_K as inward current is always positive (for $V \geq E_K$; see Fig. 6.5).

Chapter 8 treats the underlying microscopic and stochastic nature associated with the macroscopic and deterministic current. Let us for now develop our intuition by assuming that the probability of finding one activation particle in its *permissive* or open state is n (and it will be with probability $1 - n$ in its *non-permissive* or close state where no current flows through the conductance). Eq. 6.4 states that in order for the channel to be open, the four gating particles must simultaneously be in their open states. We can also think of n as the proportion of particles in their *permissive* state; potassium current can only flow if four particles are in their permissive state.

If we assume that only these two states exist (for a single particle) and that the transition from one to the other is governed by first-order kinetics, we can write down the following reaction scheme:

$$n \underset{\alpha_n}{\overset{\beta_n}{\rightleftharpoons}} 1-n\,. \tag{6.5}$$

α_n (resp. β_n) is a voltage-dependent rate constant (in units of 1/sec), specifying how many transitions occur between the closed and the open state (resp. from the open to the closed state). Mathematically, this scheme corresponds to a first-order differential equation:

$$\frac{dn}{dt} = \alpha_n(V)(1-n) - \beta_n(V)n\,. \tag{6.6}$$

The key to Hodgkin and Huxley's model—as well as the most demanding part of their investigation—was the quantitative description of the voltage-dependency of the rate constants. Instead of using rate constants α_n and β_n, we can re-express eq. 6.6 in terms of a voltage-dependent time constant $\tau_n(V)$ and steady-state value $n_\infty(V)$ with

$$\frac{dn}{dt} = \frac{n_\infty - n}{\tau_n}\,, \tag{6.7}$$

with

$$\tau_n = \frac{1}{\alpha_n + \beta_n}\,, \tag{6.8}$$

and

$$n_\infty = \frac{\alpha_n}{\alpha_n + \beta_n}\,. \tag{6.9}$$

Both descriptions, in terms of either rate constants α_n and β_n or in terms of a time constant τ_n and steady-state variable n_∞, are equivalent. While Hodgkin and Huxely used the former we will use the latter, due to its simpler physical interpretation.

One of the most striking properties of the squid membrane is the steepness of the relation between conductance and membrane potential. Below about 20 mV, the steady-state potassium membrane conductance G_K increases e-fold by varying V by 4.8 mV, while the voltage sensitivity of the sodium conductance is even higher (an e-fold change for every 3.9 mV). For higher levels of depolarization, saturation in the membrane conductance sets in (Hodgkin and Huxley, 1952a). This steep relationship must be reflected in the voltage dependency of the rate constants. Hodgkin and Huxley (1952d) approximated the voltage-dependencies of the rate constants by

$$\alpha_n(V) = \frac{10-V}{100(e^{(10-V)/10}-1)}\,, \tag{6.10}$$

and

$$\beta_n(V) = 0.125e^{-V/80}\,, \tag{6.11}$$

where V is the membrane potential relative to the axon's resting potential in units of millivolt. Fig. 6.3 shows the voltage-dependency of the associated time constant and steady-state value of the potassium activation variable. While τ_n has a bell-shaped dependency, n_∞ is

a monotonic increasing function of the membrane potential. The curve relating the steady-state potassium conductance to the membrane potential is an even steeper function, given the fourth power relationship between G_K and n. This is a hallmark of almost all ionic conductances: depolarizing the membrane potential increase their effective conductance[2]. One of the few exceptions is the appropriately named *anomalous rectifier* current, I_{AR} (frequently also termed *inward rectifier*) that turns on with increasing membrane hyperpolarization (Spain *et al.*, 1987).

The fraction of the steady-state potassium conductance open at any particular voltage $\overline{V}$, *i.e.* for $t \to \infty$, is identical to $n_\infty(\overline{V})^4$. At V_{rest} this number is very small, $n_\infty(0)^4$ =0.01, that is only about 1% of the total potassium conductance is activated! Using the voltage-clamp setup, we now move as rapidly as possible the membrane potential to $\overline{V}$ and clamp it there. The evolution of the potassium conductance is dictated by the differential eq. 6.7:

$$n(t)^4 = \left(n_\infty - (n_\infty - n_0)e^{-t/\tau_n(\overline{V})}\right)^4 , \tag{6.12}$$

where n_0 is the initial value of the potassium activation, $n_0 = n_\infty(0)$=0.32 and n_∞ its final value, $n_\infty = n_\infty(\overline{V})$. The time course of any one activation variable follows an exponential, a reflection of the underlying assumption of a first-order kinetic scheme. The time course of the fourth power of $n(t)$ is plotted on the right hand of Fig. 6.4 following a sudden shift in the membrane potential, from rest to the various voltage values indicated. Superimposed are the experimentally measured values of the potassium conductance. It is remarkable how well the points fall onto the curve. Upon stepping back to the original membrane potential, n slowly relaxes back to its original low value.

6.2.2 The Sodium Current I_{Na}

As can be seen on the left hand side of Fig. 6.4, the dynamics of the sodium conductance that we will explore now are substantially more complex.

In order to fit the kinetic behavior of the sodium current, Hodgkin and Huxley had to postulate the existence of a sodium activation particle m as well as an *inactivation particle* h:

$$I_{Na} = \overline{G}_{Na} m^3 h (V - E_{Na}) , \tag{6.13}$$

where the maximal sodium conductance $\overline{G}_{Na}$ = 120 mS/cm^2 and the sodium reversal potential E_{Na} =115 mV relative to the axon's resting potential. m and h are dimensionless numbers, with $0 \le m, h \le 1$. By our convention the sodium current is negative, *i.e.* inward, throughout the physiological voltage range (for $V < E_{Na}$; see Fig. 6.5).

The amplitude of the sodium current is contingent on four hypothetical gating particles making independent, first-order transitions between an open and a closed state. Since these particles are independent, the probability for the three m and the one h particle to exist in this state is m^3h. Notice that h is the probability that the inactivating particle is *not* in

[2]Whether or not the associated ionic current also increases depends on the relevant ionic reversal potential (eq. 6.3).

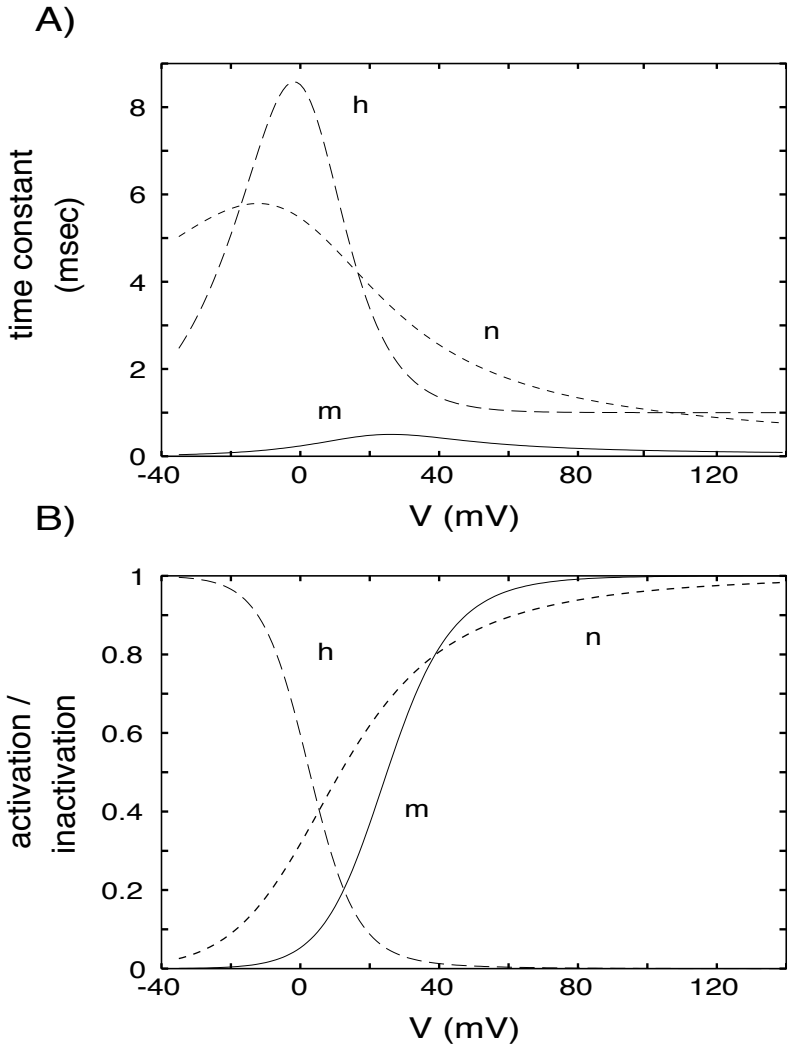

Figure 6.3: VOLTAGE DEPENDENCY OF THE GATING PARTICLES
Time constants **(A)** and steady-state activation and inactivation **(B)** as a function of the relative membrane potential V for sodium activation m (solid line) and inactivation h (dashed line) and potassium activation n (dotted line). The steady-state sodium inactivation h_∞ is a monotonic decreasing function of V, while the activation variables n_∞ and m_∞ increase with the membrane voltage. The activation of the sodium and potassium conductances are much steeper functions of the voltage, due to the power-law relationship between the activation variables and the conductances. Around rest, G_{Na} increases e-fold for every 3.9 mV and G_K for every 4.8 mV. Activating the sodium conductance occurs approximately ten times faster than inactivating sodium or activating the potassium conductance. The time constants are slowest around the resting potential.

---

its inactivating state. Formally, the temporal change of these particles is described by two

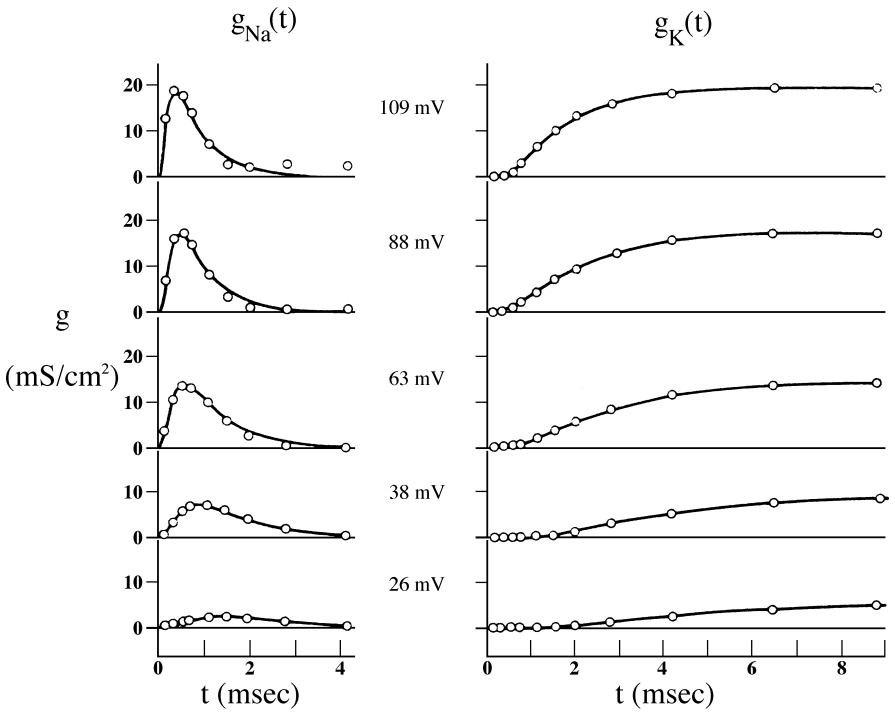

Figure 6.4: K^+ AND Na^+ CONDUCTANCES DURING A VOLTAGE STEP
The experimentally recorded (circles) and the theoretically calculated (smooth curves) changes in G_{Na} and G_K in the squid giant axon at 6.3° C during depolarizing voltage steps away the resting potential (which is here, as throughout this chapter, set to zero). For large voltage changes, G_{Na} briefly increases before it decays back to zero (due to *inactivation*), while G_K remains activated. From Hodgkin (1958).

---

first-order differential equations:

$$\frac{dm}{dt} = \alpha_m(V)(1-m) - \beta_m(V)m\,. \tag{6.14}$$

and

$$\frac{dh}{dt} = \alpha_h(V)(1-h) - \beta_h(V)h\,. \tag{6.15}$$

Empirically, Hodgkin and Huxley derived the following equations for the rate constants

$$\alpha_m(V) = \frac{25-V}{10(e^{(25-V)/10}-1)} \tag{6.16}$$

$$\beta_m(V) = 4e^{-V/18} \tag{6.17}$$

$$\alpha_h(V) = 0.07e^{-V/20} \tag{6.18}$$

$$\beta_h(V) = \frac{1}{e^{(30-V)/10}+1}\,. \tag{6.19}$$

The associated time constants and steady-state variables are plotted in Fig. 6.3 as a function of voltage. Similar to before, both τ_m[3] and τ_h are bell-shaped curves. While m_∞ is a monotonic increasing function of V as expected of an activation variable, h_∞ decreases with increasing membrane depolarization, the defining feature of an inactivating particle. It is also important to note the ten-fold difference in the kinetics of activation and inactivation at all potentials. Without inactivation, the sodium conductance would increase in response to a depolarizing voltage step within a millisecond to its new value and remain there, and would equally rapidly decay back to its old value once the voltage clamp command is removed. We defer the probabilistic interpretation of the rate constants to chapter 8.

The fraction of the steady-state sodium conductance open at rest is less than 1% of the peak sodium conductance. Inspection of Fig. 6.3 immediately reveals the reason: for voltages below or close to the resting potential of the axon, the activation variable m is close to zero while at positive potentials the inactivation variable h is almost zero. Thus, the steady-state sodium current $\overline{G}_{Na} m_\infty^3 h_\infty (V - E_{Na})$, also known as the *window current*, is always very small. The secret to obtaining the large sodium current needed to rapidly depolarize the membrane lies in the temporal dynamics of m and h. At values of the membrane close to the resting potential, h takes on a value close to one. When a sudden depolarizing voltage step is imposed onto the membrane as in Fig. 6.4, m changes within a fraction of a millisecond to its new value close to one, while h requires five or more milliseconds to relax from its previous, high value to its new and much smaller value. In other words, two processes control the sodium conductance: activation is the rapid process that increases G_{Na} upon depolarization and outpaces inactivation, the much slower process that reduces G_{Na} upon depolarization.

6.2.3 The Complete Model

Similar to most other biological membranes, the axonal membrane contains a voltage-independent "leak" conductance, G_m, which does not depend on the applied voltage and remains constant over time. The value measured by Hodgkin and Huxley, $G_m = 0.3\,\mathrm{mS/cm^2}$, corresponds to a passive membrane resistivity of $R_m = 3333\ \Omega cm^2$. The passive component also has a reversal potential associated with it. Hodgkin and Huxley did not explicitly measure V_{rest}, but adjusted it so that the total membrane current at the resting potential V =0 is zero. In other words, V_{rest} was defined via the equation $G_{Na}(0)E_{Na}+G_K(0)E_K+G_m V_{rest}$ =0, and comes out to be +10.613 mV. The membrane capacity $C_m = 1\ \mu F cm^{-2}$. At the resting potential, the effective membrane resistance due to the presence of the sum of the leak, the potassium and the (tiny) sodium conductances amounts to 857 Ωcm^2, equivalent to an effective "passive" membrane time constant of about 0.85 msec.

We can now write down a single equation for all the currents flowing across a patch of axonal membrane

$$C_m \frac{dV}{dt} = \overline{G}_{Na} m^3 h (E_{Na} - V) + \overline{G}_K n^4 (E_K - V) + G_m (V_{rest} - V) + I_{inj}(t)\,, \qquad (6.20)$$

[3]Note that the voltage-dependent membrane time constant for the activation variable, τ_m, has the same symbol as the passive membrane time constant. When in doubt, we will refer to the latter simply as τ.

where I_{inj} is the current that is injected via an intracellular electrode. This nonlinear differential equation, in addition to the three, ordinary, linear, first-order differential equations specifying the evolution of the rate constants (as well as their voltage-dependencies), constitutes the four-dimensional Hodgkin and Huxley model for the space-clamped axon or for a small patch of membrane. Throughout the book, we shall refer to eq. 6.20, in combination with the rate constants (eqs. 6.7, 14 and 15) at 6.3° C as the *standard Hodgkin-Huxley membrane patch model*. In our simulations of these equations, we solve eq. 6.20 for an equipotential $30\times\ 30\times\pi\ \mu m^2$ patch of squid axonal membrane and therefore express I_m in units of nA (and not as current density).

We will explain in the following sections how this model reproduces the stereotyped sequence of membrane events that give rise to the initiation and propagation of all-or-none action potentials.

6.3 Action Potential Generation

One of the most remarkable aspect of the axonal membrane is its propensity to respond in either of two ways to brief pulses of depolarizing inward current. If the amplitude of the pulse is below a given threshold, the membrane will depolarize slightly but will return to the membrane's resting potential, while larger currents will induce a pulse-like action potential, whose overall shape is relatively independent of the stimulus required to trigger it.

Consider the effect of delivering a short (0.5 msec) inward current pulse $I_{inj}(t)$ of 0.35 nA amplitude to the membrane (Fig. 6.5). The injected current charges up the membrane capacitance, depolarizing the membrane in the process. The smaller this capacitance, the faster the potential will rise. The depolarization has the effect of slightly increasing m and n, *i.e.* increasing both sodium and potassium activation, but decreasing h, that is decreasing potassium inactivation. Because the time constant of sodium activation is more than one order of magnitude faster than τ_n and τ_h at these voltages, we can consider the later two for the moment to be stationary. But the sodium conductance, G_{Na}, will increase somewhat. Because the membrane is depolarized from rest, the driving potential for the potassium current, $V - E_K$, has also increased. The concomitant increase in I_K outweighs the increase in I_{Na} due to the increase in G_{Na} and the overall current is outward, driving the axon's potential back toward the resting potential. The membrane potential will slightly undershoot and then overshoot until it finally returns to V_{rest}. The oscillatory response around the resting potential can be attributed to the small-signal behavior of the potassium conductance acting phenomenologically similar to an inductance (see chapter 10 for a further discussion of this).

If the amplitude of the current pulse is slightly increased to 0.4 nA, the depolarization due to the voltage-independent membrane components will reach a point where the amount of I_{Na} generated exceeds the amount of I_K. At this point, the membrane voltage undergoes a run-away reaction: the additional I_{Na} depolarizes the membrane, further increasing m that increases I_{Na} and further membrane depolarization. Given the almost instantaneous dynamics of sodium activation (τ_m is $\approx$ 0.1-0.2 msec at these potentials), the inrushing

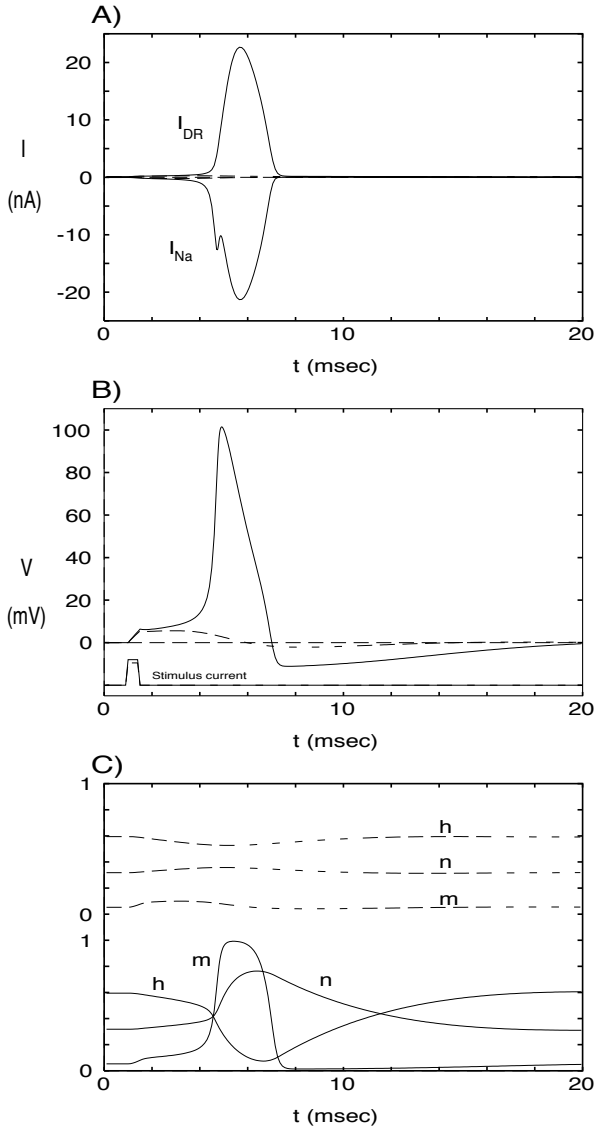

Figure 6.5: HODGKIN-HUXLEY ACTION POTENTIAL

Computed action potential in response to a 0.5 msec current pulse of 0.4 nA amplitude (solid lines) in comparison to a subtreshold response following a 0.35 nA current pulse (dashed lines). **(A)** Time-course of the two ionic currents. Note their large size compared to the stimulating current. **(B)** The membrane potential in response to threshold and subthreshold stimuli. The injected current charges up the membrane capacity (with an effective membrane time constant τ =0.85 msec), enabeling sufficient I_{Na} to be recruited to outweigh the increase in I_K (due to the increase in driving potential). The smaller current pulse fails to trigger an action potential, but causes a depolarization followed by a small hyperpolarization due to activation of I_K. The lower panel **(C)** shows the dynamics of all three gating particles. Sodium activation m changes much more rapidly than either h or n. The long time course of potassium activation n explains why the membrane potential takes 12 msec after the potential has first dipped below the resting potential to return to baseline level.

sodium current moves the membrane potential within a fraction of a millisecond to 0 mV and beyond. In the absence of sodium inactivation and potassium activation, this positive feedback process would continue until the membrane would come to rest at E_{Na}. As we saw already in Fig. 6.4, after a delay both the slower sodium inactivation variable h as well as the potassium activation n will turn on (explaining why I_K is also called the *delayed rectifier* current or I_{DR}). Sodium inactivation acts to directly decrease the amount of sodium conductance available, while the activation of the potassium conductance tends to try to bring the axon's membrane potential toward E_K by increasing I_K. Thus, both processes cause the membrane potential to dip down from its peak. Because the total sodium current quickly falls to zero after 1 msec, but I_K persists longer at small amplitudes (not readily visible in Fig. 6.5) the membrane potential is depressed to below its resting level, that is the axon *hyperpolarizes*. At these low potentials, eventually potassium activation switches off, returning the system to its initial configuration as V approaches the resting potential.

6.3.1 The Voltage Threshold for Spike Initiation

What are the exact conditions under which a spike is initiated? Does the voltage have to exceed a particular threshold value V_{th}, or does a minimal amount of current I_{th} have to be injected, or does a certain amount of electrical charge Q_{th} have to be delivered to the membrane in order to initiate spiking? These possibilities and more have been discussed in the literature and experimental evidence exists to support all of these views under different circumstances (Hodgkin and Rushton, 1946; Cooley, Dodge and Cohen, 1965; Noble and Stein, 1966; Cole, 1972; Rinzel, 1978a; for a thorough discussion see Jack *et al.*, 1975). Because the squid axon is not a good model for spike encoding in central neurons, we will defer a more detailed discussion of this issue to sections 17.3 and 19.1. We here limit ourselves to considering spike initiation in an idealized nonlinear membrane, without dealing with the complications of cable structures (such as the axon).

To answer this question, we need to consider the current-voltage relationship of the squid axonal membrane. Because we are interested in rapid synaptic inputs, we assume that the rise-time of the synaptic current is faster than the effective passive time constant, $\tau = 0.85$ msec and make use of the observation that the dynamics of sodium activation m is very rapid (the associated time constant is always less than 0.5 msec) and at least a factor of ten faster than sodium inactivation h and potassium activation n (see Fig. 6.3). With these observations in mind, we ask what happens if the input very rapidly depolarizes the membrane to a new value V? Let us estimate the current that will flow with the help of the *instantaneous* current-voltage relationship $I_0(V)$ (Fig. 6.6).

I_0 is given by the sum of the ionic and the leak currents. We approximate the associated sodium and potassium conductances by assuming that h and n have not had time to change from the value they had at the resting potential $V = 0$, while m adjust instantaneously to its new value at V. In other words,

$$I_0(V) = \overline{G}_{Na} m(V)^3 h(0)(V - E_{Na}) + \overline{G}_K n(0)^4 (V - E_K) + G_m (V - V_{rest}) \,. \qquad (6.21)$$

Fig. 6.6 shows the inverted U-form shape of I_0 in the neighborhood of the resting potential, as well as its three ionic components, I_{Na}, I_K and I_{leak}.

In the absence of any input, the system rests at V =0. If a small, depolarizing voltage step is applied, the system is displaced to the right, generating a small, positive current. This current is outward since the increase in m (increasing the amplitude of I_{Na}) is outweighed by the increase in the driving potential $V - E_K$ (increasing I_K). This forces the membrane potential back down towards the resting potential: the voltage trajectory corresponds to a subthreshold input. Similarly, if an hyperpolarizing current step is injected, moving the system to below V =0, a negative, inward current is generated, pulling the membrane back up towards V_{rest}. The slope of the I-V curve around the resting potential, $\partial I/\partial V$, termed the *membrane slope conductance* (for a substantial discussion of this concept, see section 17.1.2) is positive. That is, the point V =0 is a *stable attractor* (for these and related notions, we defer the reader to the following chapter).

$I_0(V)$ has a second zero-crossing at $V = V_{th} \approx 2.5$ mV. If an input moves the membrane potential to exactly V_{th}, no current flows and the system remains at V_{th} (Fig. 6.6). Because the slope conductance is negative, the point is unstable and an arbitrarily small perturbation will carry the system away from the zero-crossing. A negative perturbation will carry the system back to V_{rest}. Conversely, a positive voltage displacement, no matter how minute, causes a small, inward current to flow that further depolarizes the membrane (due to the negative slope conductance), leading in turn to a larger inward current and so on. The membrane potential rapidly increases to above zero, that is an action potential is triggered. During this phase, very large inward currents are generated, far exceeding the amplitude of the modest stimulus current (recall that around these potentials, I_{Na} increases e-fold every 3.9 mV). For the patch of squid membrane simulated here (where the current scales linearly with the area of the patch), the peak of I_{Na} is about 23 nA.

This qualitative account of the origin of the voltage threshold for an active patch of membrane argues that in order for an action potential to be initiated, the net inward current must be negative. For rapid input, this first occurs at $V = V_{th}$. This analysis was based on the rather restrictive assumption that m changes instantaneously, while h and n remain fixed. In practice, neither assumption is perfect. Indeed, while our argument predicts V_{th} =2.5 mV, the voltage threshold for spike initiation for rapid EPSPs for the Hodgkin-Huxley equation is, in fact, equal to 6.85 mV (Noble and Stein, 1966). As discussed in section 17.3, reaching a particular value of the voltage for a rapid input in a single compartment is equivalent with rapidly dumping a threshold amount of charge Q_{th} into the system.

Applying a current step that increases very slowly in amplitude—allowing the system to always relax to its stationary state—prevents any substantial sodium current from flowing and will therefore not cause spiking. Thus, not only does a given voltage threshold has to be reached and exceeded but also within a given time window. We take up this issue in section 17.3 in the context of our full pyramidal cell model and in section 19.1 to explore how V_{th} is affected by the cable structure. For the pyramidal cell model, both V_{th} as well as I_{th} can be estimated quite accurately from the sustained and the instantaneous current-voltage relationships.

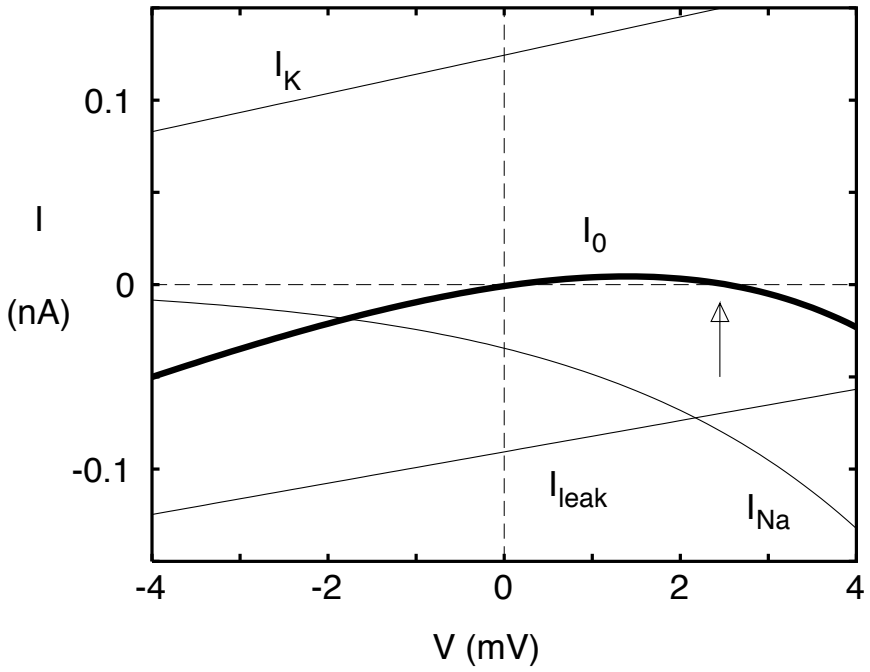

Figure 6.6: CURRENT-VOLTAGE RELATIONSHIP AROUND REST
The instantaneous I-V relationship I_0 associated with our standard patch of squid axon membrane and its three components: $I_0 = I_{Na} + I_K + I_{leak}$ (eq. 6.21). Because m changes much faster than either h or n for rapid inputs, we computed G_{Na} and G_K under the assumption that m adapts instantaneously to its new value at V, while h and n remain at their resting values. I_0 crosses the voltage axis at two points: a stable point at V =0 and an unstable one at $V_{th} \approx$ 2.5 mV. Under these idealized conditions, any input that exceeds V_{th} will lead to a spike. For the "real" equations, m does not change instantaneously and nor do n and h remain stationary; thus, I_0 only crudely predicts the voltage threshold which is, in fact, 6.85 mV for rapid synaptic input. Note that I_0 is specified in absolute terms and scales with the size of the membrane patch.

6.3.2 Refractory Period

The nervous system needs to rapidly repolarize the membrane potential following its 100 mV excursion from the resting potential. Given a specific membrane capacitance of 1 μm F/cm^2, this amounts to transferring about 6,000 positively charged ions per μm^2 of membrane area.

The way this is accomplished is by increasing a potassium conductance, G_K. This conductance remains activated even subsequent to spike polarization (up to 12 msec following the peak of the action potential in Fig. 6.5), causing the membrane to undergo a hyperpolarization. During this period, it is more difficult to initiate an action potential than before; the membrane remains in a *refractory* state. The reason for the reduced ability of the membrane to discharge again is the inactivation of I_{Na} (*i.e.* h is small) and the continuing activation of I_K (n only decays slowly).

This *refractory period* can be documented by the use of a second current pulse (Fig. 6.7). At t =1 msec a 0.5 msec current pulse is injected into our standard patch of squid axonal membrane. The amplitude of this pulse, I_1 =3.95 nA, is close to the minimal one needed to generate an action potential. The input causes a spike to be triggered that peaks at around 5 msec and repolarizes to V =0 at t =7 msec. This time, at which the membrane potential starts to dip below the resting potential (Fig. 6.5), is somewhat arbitrarily assigned to Δt =0. Following this point, a second 0.5 msec long current pulse of amplitude I_2 is applied Δt msec later. The amplitude of I_2 is increased until a second action potential is generated. This first occurs at Δt =2 msec (that is 2 msec after the membrane potential has repolarized to zero). At this time, I_2/I_1 =23.7, that is the amplitude of the second pulse must be 23.7 times larger than the amplitude of the first pulse in order to trigger a spike. Since such large current amplitudes are unphysiological, the membrane is *de facto* not excitable during this period that is frequently referred to as the *absolute refractory period*. Up to 11 msec after repolarization of the membrane due to the first spike is the threshold for initiation of the second spike elevated (*relative refractory period*; Fig. 6.7). This is followed by a brief period of mild hyperexcitability when a spike can be elicited by a slightly (15%) smaller current than under resting conditions.

¿From a computational point of view, it is important to realize that the threshold behavior of the Hodgkin and Huxley model depends on the previous spiking history of the membrane. In the squid axon, as in most axons, the threshold rises only briefly, returning to baseline levels after 20 msec or less. As warming the axon to body temperatures speeds up the rates of gating two- to fourfold[4], the minimal separation times is expected to be only 1-2 msec for axons in warm blooded animals. Nerve cells—as compared to axons— often display a much longer increase in their effective spiking threshold, depending on the number of action potentials generated within the last 100 or more milliseconds (Raymond, 1979). Section 9.2.3 will treat the biophysical mechanism underlying this short-term *firing frequency adaptation* in more detail.

[4]A crucial parameter in determining the dynamics of the action potential is the temperature T. As first mentioned in a footnote in section 4.6.1, if the temperature is reduced, the rate at which the ionic channels underlying the action potential open or close slows down, while the peak conductance remains unchanged. Hodgkin and Huxley recorded most of their data at 6.3° C and the rate constants are expressed at these temperatures (eqs. 6.10, 11 and 6.16 through 6.19). To obtain the action potential at any other temperature T, all α's and β's all need to be corrected by $Q_{10}^{(T-6.3)/10}$, with a Q_{10} between $2-4$ (Hodgkin, Huxley and Katz, 1952; Beam and Donaldson, 1983; for a definition of Q_{10} see the footnote in section 4.6). The Q_{10} for the peak conductances is a modest 1.3. As the temperature is increased, the *upstroke*, *i.e.* the rate at which the voltage rises during the rapid, depolarizing phase of the action potential, increases, because the speed at which I_{Na} is activated increases. At the same time, both sodium inactivation as well as potassium activation increases. Altogether, the total duration of the spike decreases. At temperatures above 33° C no spike is generated (Hodgkin and Katz, 1949; of course, the squid axon lives in far more frigid waters than these balmy temperatures).

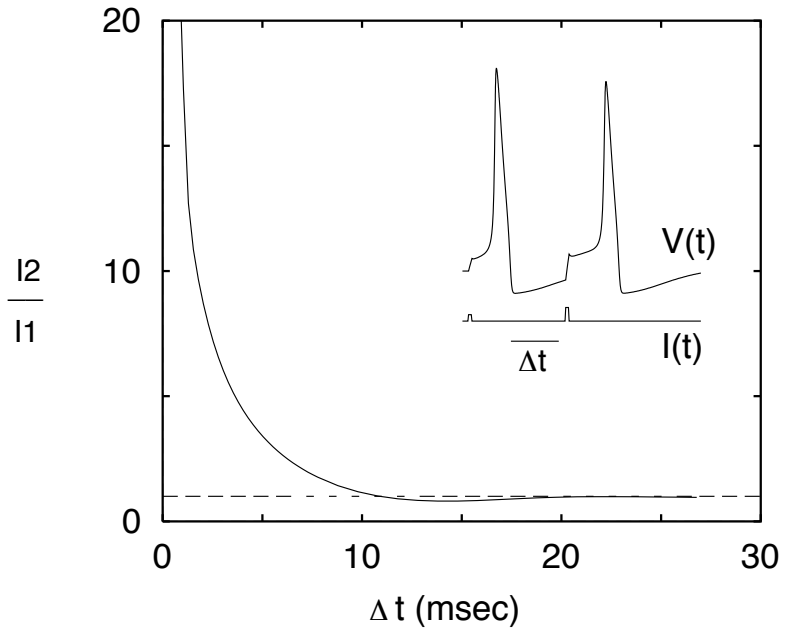

Figure 6.7: Refractory Period
A 0.5 msec brief current pulse of I_1 =0.4 nA amplitude causes an action potential (Fig. 6.5). A second, equally brief, pulse of amplitude I_2 is injected Δt msec after the membrane potential due to the first spike has reached V =0 and is about to hyperpolarize the membrane. For each value of $\Delta t, I_2$ is increased until a second spike is generated (see the inset for Δt =10 msec). The ratio I_2/I_1 of the two pulses is here plotted as a function of Δt. For several milliseconds following repolarization, the membrane is practically inexcitable since such large currents are unphysiological (*absolute refractory period*). Subsequently, a spike can be generated but it requires a larger current input (*relative refractory period*). This is followed by a brief period of reduced threshold (hyperexcitability). No more interactions are observed beyond about Δt =18 msec.

6.4 Relating Firing Frequency to Sustained Current Input

What happens if a long-lasting current step of constant amplitude is injected into the space-clamped axon (Agin, 1964; Cooley, Dodge and Cohen, 1965; Stein, 1967a)? If the current is too small, it will give rise to a persistent sub-threshold depolarization (Fig. 6.8). Plotting the steady-state membrane depolarization as a function of the applied membrane current (Fig. 6.9A) reveals the linear relationship between the two. If the input is of sufficient amplitude to exceed the threshold, the membrane will generate a single action potential (Fig. 6.8). The minimal amount of sustained current needed to generate at least one action potential (but not necessarily an infinite train of spikes) is called *rheobase* (Cole, 1972). For our standard membrane patch, rheobase corresponds to 0.065 nA (this current is obviously far

less than the amplitude of the brief current pulse used previously). After the spike has been trigged and following the afterhyperpolarization, $V(t)$ stabilizes at around 2 mV positive to the resting potential, limiting the removal of sodium inactivation as well as enhancing I_K. As the current amplitude is increased, the offset depolarization following the action potential and its hyperpolarization increases until, when the amplitude of the current step is about three times rheobase (0.175 nA), a second action potential is initiated. At around 0.18 nA (I_1 in Fig. 6.9A) the membrane will generate an indefinite train of spikes at fixed intervals: the membrane potential between action potentials always slowly creeps past V_{th} and the cycle begins anew: the system travels on a stable limit cycle. In a noiseless situation, the interval between consecutive spikes is constant and the cell behaves as a periodic oscillators with constant frequency.

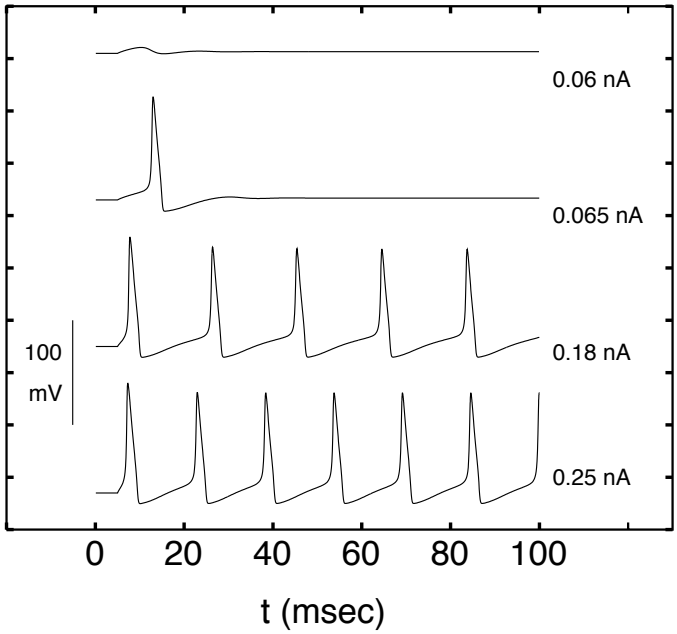

Figure 6.8: Repetitive Spiking

Voltage trajectories in response to current steps of various amplitudes in the standard patch of squid axonal membrane. The minimum sustained current necessary to initiate a spike, termed *rheobase*, is 0.065 nA. In order for the membrane to spike indefinitely, larger currents must be used. Experimentally, the squid axon usually stops firing after a few seconds due to secondary inactivation processes not modeled by the Hodgkin and Huxley (1952d) equations.

Fig. 6.9A shows the associated steady-state voltage-current relationship. Experimentally, it can be obtained by clamping the membrane potential to a particular value V and by measuring the resultant clamp current I. The equations generate infinite trains of action potentials for $I \geq I_1$ (dashed line in Fig. 6.9A).

If the current amplitude is further increased, the interspike intervals begin to decrease and the spiking frequency increases. Fig. 6.9B shows the relationship between the amplitude

of the injected current and the spiking frequency around threshold and Fig. 6.10A over a larger current range. It is referred to as the *frequency-current* or f-I curve. Overall, there is a fairly limited range of frequencies at which the membrane fires, between 53 and 138 Hz. If a current at the upper amplitude range is injected in the axon, the membrane fails to repolarize sufficiently between spikes to relieve sodium inactivation. Thus, although the membrane potential does show oscillatory behavior, no true action potentials are generated.

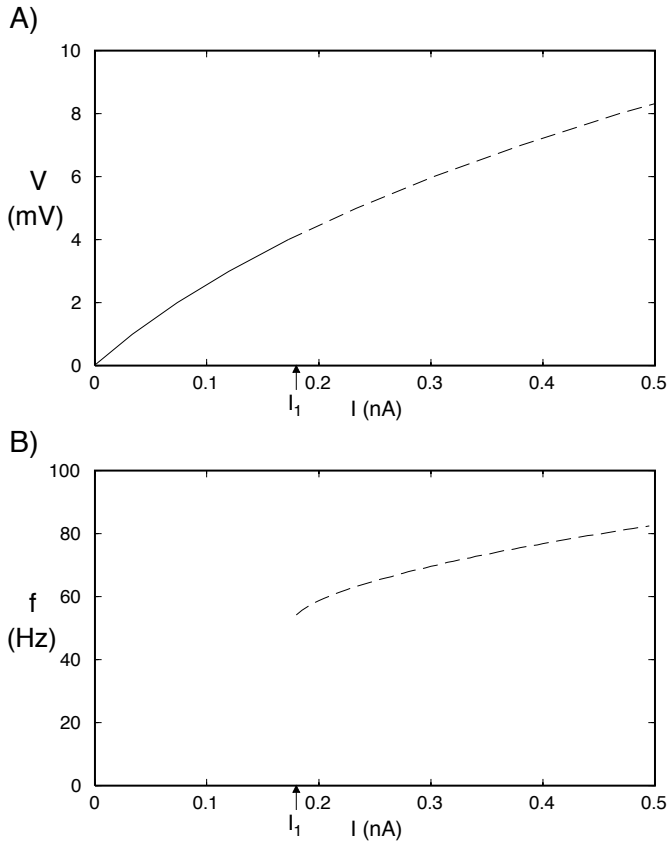

Figure 6.9: SUSTAINED SPIKING IN THE HODGKIN-HUXLEY EQUATIONS
(A) Steady-state voltage-current relationship and **(B)** the f-I or discharge curve as a function of the amplitude of the sustained current I associated with the Hodgkin-Huxley equations for a patch of squid axonal membrane. For currents less than 0.18 nA, the membrane responds by a sustained depolarization (solid curve). At I_1, the system loses its stability and generates an infinite train of action potentials: it moves along a stable limit cycle (dashed line). A characteristic feature of the squid membrane is its abrupt onset of firing with non-zero oscillation frequency. The steady-state V-I curve can also be viewed as the sum of all steady-state ionic currents flowing at any particular membrane potential V_m.

Some authors (Hagiwara and Oomura, 1958) have been unable to reproduce maintaining firing experimentally (see, however, Chapman, 1966). This is most likely due to secondary

inactivation mechanisms which are not treated by the Hodgkin and Huxley equations. Yet for shorter times, the theoretical model of Hodgkin and Huxley makes reasonably satisfactory predictions of the behavior of the space-clamped axon (for a detailed comparison between experimental observations and theoretical predictions see Guttman and Barnhill, 1970), in particular with respect to the small dynamic range of firing frequencies supported by the axonal membrane and the abrupt onset of spiking at a high firing frequency. The f-I curve can be well approximated by either an square root or a logarithmic relationship between frequency and injected current (Agin, 1964; see Fig. 6.10).

In general, the f-I curves of neurons show a sigmoidal behavior for large input values. This justifies the introduction of a smooth, sigmoidal-type of nonlinearity mimicking the neuronal input-output transduction process in continuously valued neural network models (Hopfield, 1984). It is important to keep in mind that the paradigm under which the f-I curves are obtained, sustained current input, represents only a very crude approximation to the dynamic events occurring during synaptic bombardment of a cell leading to very complex spike discharge patterns (see chapter 15).

An important feature of the Hodgkin and Huxley model is that the frequency at the onset of repetitive activity has a well-defined non-zero minimum (about 53 Hz at 6.3° C; Fig. 6.10B). The membrane is not able to sustain oscillations at lower frequencies. This behavior, generated by a so-called *Hopf bifurcation* mechanism, is generic to a large class of oscillators occurring in nonlinear differential equations (Cronin, 1987; Rinzel and Ermentrout, 1989) and will be treated in more detail in the following chapter.

As first explicitly simulated by Stein (1967b), adding random variability to the input can increase the bandwidth of the axon by effectively increasing the range within which the membrane can generate action potentials. If the input current is made to vary around its mean with some variance, reflecting for instance the spontaneous release of synaptic vesicles, the sharp discontinuity in the firing frequency at low current amplitudes is eliminated, since even with an input current that is on average below threshold, the stimulus will become strong enough to generate an impulse with a finite, though small, average frequency. Depending on the level of noise, the effective minimal firing frequency can be reduced to close to zero (Fig. 6.10B). A similar linearization behavior can be obtained if the continuous, deterministic and macroscopic currents inherent in the Hodgkin-Huxley equations are approximated by the underlying discrete, stochastic and microscopic channels (Skaugen and Walloe, 1979; see section 8.3).

Adding noise to a quantized signal to reduce the effect of this discretization is a standard technique in engineering known as *dithering* or *stochastic linearization* (Gammaitoni, 1995; Stemmler, 1996).

A large number of neurons can generate repetitive spike trains with arbitrarily small frequencies. As first shown by Connor and Stevens (1971c) in their Hodgkin and Huxley-like model of a gastropod nerve cell, addition of a transient, inactivating potassium current (termed the I_A current) enables the cell to respond to very small sustained input currents with a maintained discharge of very low frequency (this topic will be further pursued in section 7.2.2). Such low firing frequency are also supported by pyramidal cells (Fig. 9.7).

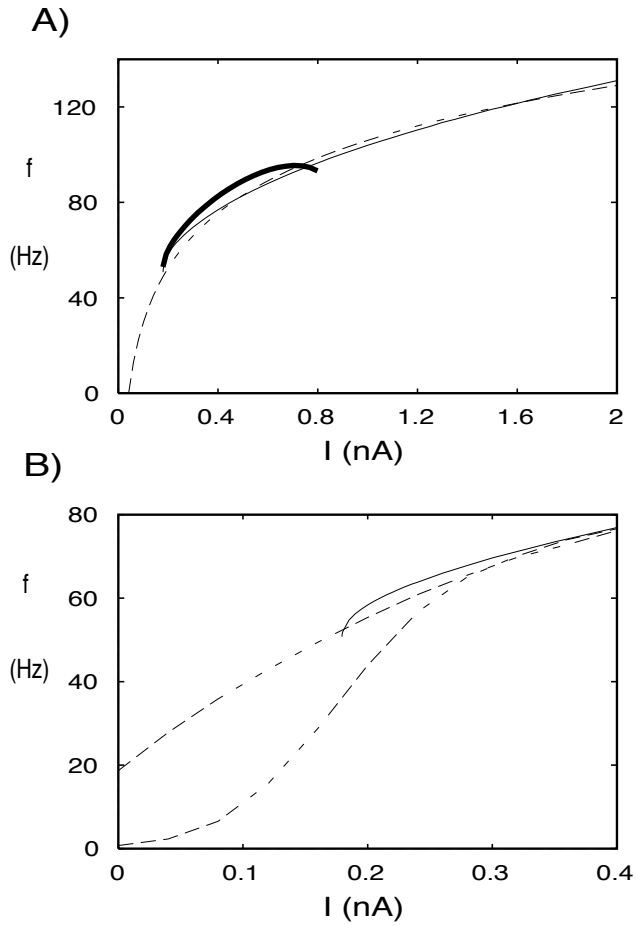

Figure 6.10: The Hodgkin-Huxley f-I curve and Noise
(A) The relationship between the amplitude of an injected current step and the frequency of the resultant sustained discharge of action potentials (f-I curve) for a membrane patch of squid axon at 6.3° C (solid line) and its numerical fit (dashed line) by $f = 33.2 \log I + 106$. Superimposed in bold is the f-I curve for the standard squid axon cable (using normalized current). Notice the very limited bandwidth of axonal firing. **(B)** The f-I curve for the membrane patch case around its threshold (rheobase) in the presence of noise. White (2000 Hz band-limited) current noise whose amplitude is Gaussian distributed with zero mean current is added to the current stimulus. In the absence of any noise (solid line) the f-I curve shows abrupt onset of spiking. The effect of noise (the lower dashed curve has a standard deviation of 0.05 nA and the upper dotted curve of 0.1 nA) is to linearize the threshold behavior and to increase the bandwidth of transmission (stochastic linearization). Linear f-I curves are also obtained when replacing the continuous and deterministic Hodgkin-Huxley currents by discrete and stochastic channels (see section 8.3).

6.5 Action Potential Propagation Along the Axon

Once the threshold for excitation has been exceeded, the all-or-none action potential can propagate from the stimulus site to other areas of the axon. The hypothesis that this

propagation is mediated by cable currents flowing from excited to neighbouring, non-excited regions was suggested already around the turn of the century by Hermann (1899). It was not until Hodgkin (1937) that direct experimental proof became available. A quantitative theory of this propagation had to await Hodgkin and Huxley's 1952 study. Because this has been a very well explored chapter in the history of biophysics, we will be brief here, only summarizing the salient points. Chapter 10 in Jack *et al.* (1975) provides a deep and thorough coverage of nonlinear cable theory as applied to the conduction of action potentials. Section 19.1 will deal with how cable structures, such as an infinite cylinder, affect the voltage threshold for spike initiation.

6.5.1 The Empirical Determination of the Propagation Velocity

The equivalent electrical circuit replicates the patch of sodium, potassium and leak conductances and batteries of Fig. 6.2 along the cable in a fashion we are already familiar with from the passive cable (Fig. 6.12). Eq. 2.5 specifies the relationship between the membrane current (per unit length) and the voltage along the cable:

$$i_m = \frac{1}{r_a}\frac{\partial^2 V}{\partial x^2}\,. \tag{6.22}$$

In eq. 6.20, we derived the membrane current (per unit area) flowing in a patch of axonal membrane. Combining the two with the appropriate attention to scaling factors leads to an equation relating the potential along the axon to the electrical property of the active membrane:

$$\frac{d}{4R_i}\frac{\partial^2 V}{\partial x^2} = C_m\frac{\partial V}{\partial t} + \overline{G}_{Na}m^3h(V-E_{Na}) + \overline{G}_K n^4(V-E_K) + G_m(V-V_{rest})\,, \tag{6.23}$$

where d is the diameter of the axon. Hodgkin and Huxley (1952d) used a d =0.476 mm thick axon in their calculations and a value of $R_i = 35.4\ \Omega cm$. This nonlinear partial differential equation, in conjunction with the three equations describing the dynamics of m, h and n and the appropriate initial and boundary conditions, constitutes the complete Hodgkin and Huxley model.

This type of second-order equation, for which no general, analytical solution is known, is called a *reaction-diffusion* equation, because it can be put into the form of

$$\frac{\partial V}{\partial t} = D\frac{\partial^2 V}{\partial x^2} + F(V)\,, \tag{6.24}$$

with $D > 0$ constant. We will meet this type of equation again when considering the dynamics of intracellular calcium (see chapter **??**). Under certain conditions, it has wave-like solutions.

Because Hodgkin and Huxley only had access to a very primitive hand calculator, they could not directly solve eq. 6.23. Instead, they considered a particular solution to these equations. Since they observed that the action potential propagated along the axon without

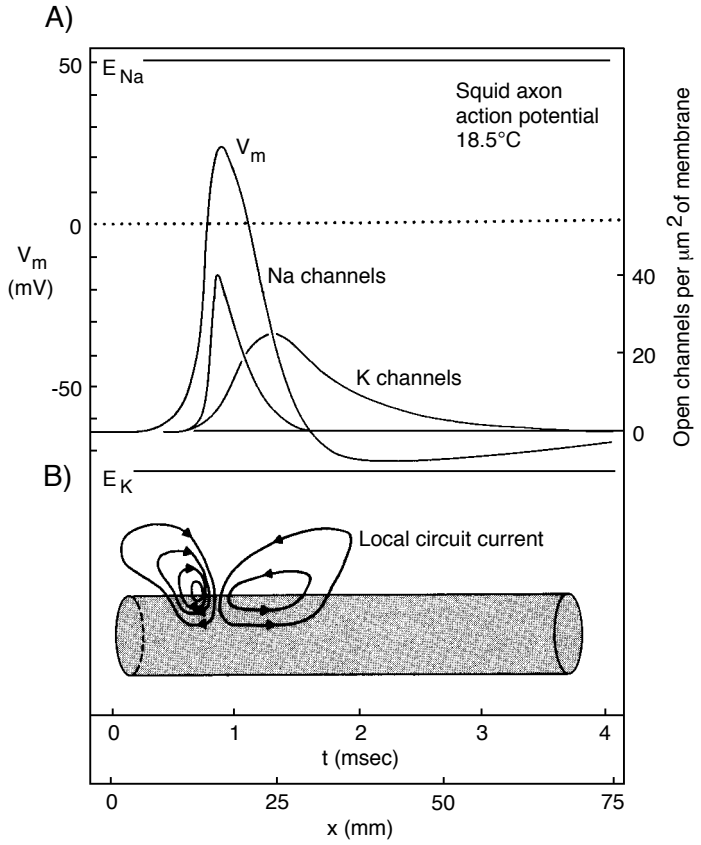

Figure 6.11: The Local Circuit Current in the Squid Axon
Illustration of the events occuring in the squid axon during the propagation of an action potential. Since the spike behaves like a wave traveling at constant velocity, these two panels can be thought of as either showing the voltage and currents in time at one location or as providing a snapshot of the state of the axon at one particular instant (see the space/time axes at the bottom). **(A)** The distribution of the voltage (left scale) or the number of open channels (right scale) as inferred from the Hodgkin and Huxley model at 18.5° C. **(B)** The *local circuit currents* that spread from an excited patch of the axon to neighbouring regions bringing them above threshold, thereby propagating the action potential. The diameter of the axon (0.476 mm) is not drawn to scale. ¿From Hille (1992).

---

changing its shape, they postulated the existence of a wave solution to this equation, in which the action potential travels with constant velocity u along the axon, *i.e.* $V(x,t) = V(x-ut)$. Taking the second spatial and temporal derivative of this expression and using the chain rule leads to a second-order hyperbolic partial differential equation

$$\frac{\partial^2 V}{\partial x^2} = \frac{1}{u^2}\frac{\partial^2 V}{\partial t^2}\,. \tag{6.25}$$

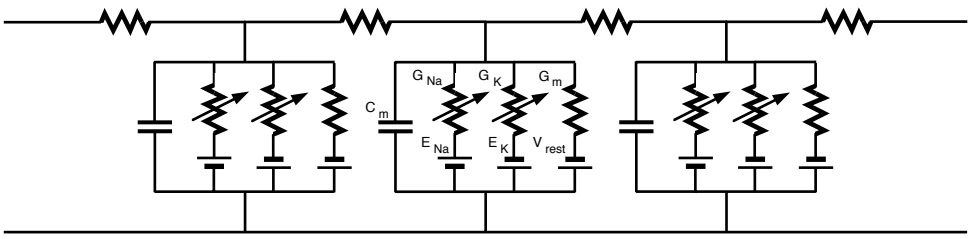

Figure 6.12: ELECTRICAL CIRCUIT OF THE SQUID GIANT AXON
One-dimensional cable model of the squid giant axon. The structure of the cable is as in the passive case (Fig. 2.2B), with the RC membrane components augmented with circuit elements modeling the sodium and potassium current (Fig. 6.2).

Replacing the second spatial derivative term in eq. 6.23 with this expression yields

$$\frac{1}{K}\frac{d^2V}{dt^2} = \frac{dV}{dt} + \frac{I_i}{C_m}, \tag{6.26}$$

with $K = 4R_i u^2 C_m/d$ and I_i a shorthand for the two ionic and the leak current. Eq. 6.26 is an ordinary second-order differential equation, whose solution is much easier to compute than the solution to the full-blown partial differential equation. It does, require, though, a value for u. By a laborious trial and error procedure, Hodgkin and Huxley iteratively solved this equation until they found a value of u leading to a stable propagating wave solution. In a truly remarkable test of the power of their model, they estimated 18.8 m/sec (at 18.3° C) for the velocity at which the spike propagates along the squid giant axon, a value within 10% of the experimental value of 21.2 m/sec. This is all the more remarkable, given that their model is based on voltage- and spaced-clamp data, and represents one of the rare instances in which a neurobiological model makes a successful quantitative prediction!

We can establish the dependency of the velocity on the diameter of the fiber using the following argumentation. Because both I_i as well as C_m are expressed as current and capacitance per unit membrane area, their ratio is independent of the fiber diameter. The voltage across the membrane and its temporal derivatives must also be independent of d. This implies that the constant K in eq. 6.26 must remain invariant to changes in diameter. Assuming that C_m and R_i do not depend on d, we are lead to the conclusion that the velocity u must be

$$u \propto \sqrt{d}. \tag{6.27}$$

In other words, the propagation velocity in unmyelinated fibers is expected to be proportional to the square root of the axonal diameter[5]. Indeed, this predicted relationship is roughly followed in real neurons (see Fig. 6.15; Ritchie, 1995).

This implies that if the delay between spike initiation at the cell body and the arrival of the spike at the termination of an axon needs to be cut in half, the diameter of the axon

[5]Notice that we derived a similar square-root relationship between diameter and "pseudo-velocity" for the decremental wave in the case of a passive cable (eq. 2.53).

needs to increase by a factor 4, a heavy price to pay for rapid communication. The premium put on minimizing propagation delay in long cable structures is most likely the reason the squid evolved such thick axons. As we will see further below, many axons in vertebrates use a particular form of electrical insulation, termed *myelination*, to greatly speed up spike propagation without a concomitant increase in fiber diameter.

It was more than ten years later that Cooley, Dodge and Cohen (1965; see also Cooley and Dodge, 1966) solved the full partial differential eq. 6.23 numerically using an iterative technique. Fig. 6.13 displays the voltage trajectory at three different locations along the axon; at x =0 a short, suprathreshold current pulse charges up the local membrane capacitance. This activates the sodium conductance and Na^+ ions rush in, initiating the full-blown action potential (not shown). The local circuit current generated by this spike leads to an exponential rise in the membrane potential in the neighbouring region, known as the "foot" of the action potential. This capacitive current in turn activates the local sodium conductance that will increase rapidly, bringing this region above threshold: the spike propagates along the axon. Different from the space-clamped axon where the capacitive current is always equal and opposite to the ionic currents once the stimulus current has stopped flowing (eq. 6.20), the time course of current is more complex during the propagated action potential due to the local circuit currents. Because some fraction of the local membrane current depolarizes neighbouring segments of the axonal cable (the so- called *local circuit* currents; see Fig. 6.11), the current amplitude required to trigger at least one action potential is larger than the current amplitude in the space-clamped case.

If the voltage applied to the squid membrane is small enough, one can *linearize* the membrane, describing its behavior in terms of voltage-independent resistances, capacitances and inductances. This procedure was first carried out by Hodgkin and Huxley (1952d) and will be discussed in detail in chapter 10. Under these circumstances, a space constant λ can be associated with the "linearized" cable, describing how very small currents are attenuated along the axon. At rest, the d.c. space constant for the squid axon is λ =5.4 mm, about ten times larger than its diameter.

When long current steps of varying amplitude are injected into the axon, the squid axon responds with regular, periodic spikes. However, the already small dynamic range of the f-I curve of the space-clamped axon (Fig. 6.10A) becomes further reduced to a factor of less than 1.7 when the the sustained firing activity in the full axon is considered (from 58 to 96 Hz at 6.3° C). Thus, while the Hodgkin and Huxley model describes to a remarkable degree the behavior of the squid's giant axon, the equations do not serve as an adequate model for impulse transduction in nerve cells, most of which have a dynamic range that extends over two orders of magnitude.

As predicted by Huxley (1959), Cooley and Dodge (1966) found a second solution to the Hodgkin and Huxley equations. At values of current input very close to the threshold for spike initiation, they observed a decremental wave propagating away from the current source. This solution quickly dies away to zero potential as x increases and is only observed if the amplitude of the current step is within 10^{-3} of the threshold current. This also reveals the fact that the Hodgkin and Huxley model does not possess a strict threshold in the true

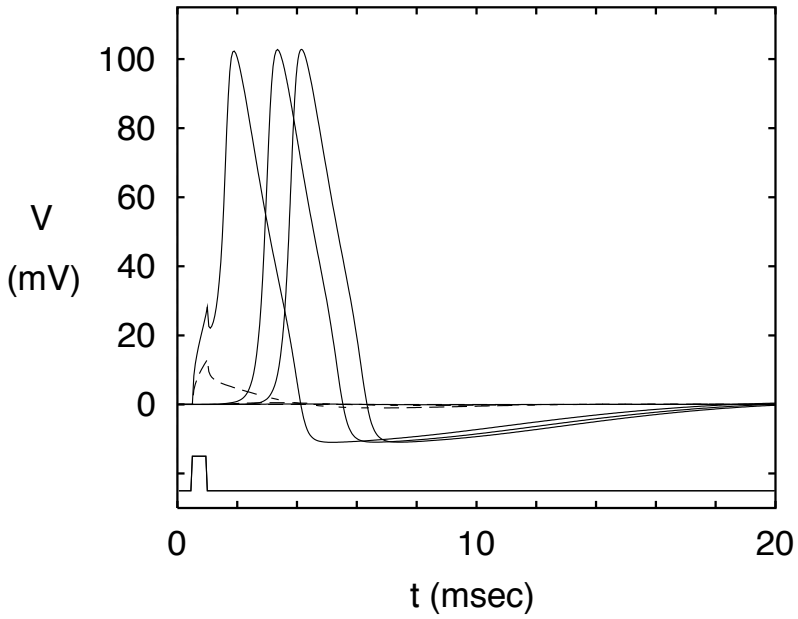

Figure 6.13: PROPAGATING ACTION POTENTIAL

The solution to the complete Hodgkin and Huxley model for a 5 cm long piece of squid axon for a brief suprathreshold current pulse delivered to one end of the axon. This pulse generates an action potential that travels down the cable and is shown here at the origin as well as 2 and 3 cm away from the stimulating electrode (solid lines). Notice that the shape of the action potential remains invariant due to the nonlinear membrane. The effective velocity of the spike is 12.3 m/sec (at 6.3° C). If the amplitude of the current pulse is halved, only a local depolarization is generated (dashed curve) that depolarizes the membrane 2 cm away by a mere 0.5 mV (not shown). This illustrates the dramatic difference between active and passive voltage propagation.

---

sense of the word. In other words, there exists a continuous transformation between the subthreshold and the threshold voltage response. Yet in order to reveal these intermediate solutions the excitation must be adjusted with a degree of accuracy impossible to achieve physiologically. Practically speaking, given unavoidable noise in any neuronal system, only the propagating wave solution (with its associated threshold) plays a significant role in propagating information along the axon.

Cooley and Dodge (1966) also considered what happens if the density of voltage-dependent channels underlying G_{Na} and G_K is attenuated by a factor of η (with $0 \leq \eta \leq 1$; the value of V_{rest} and G_{leak} were adjusted so that the resting potential and resting conductance were held constant). Reducing these conductances is somewhat analogous to the action of certain local anesthetics, such as lidocaine or procaine as used by dentists, in blocking action potential propagation. As η is reduced below one, the velocity of propagation as well as the peak amplitude of the spike are reduced. For η <0.26, no uniform wave solution is possible and the "action potential" decrements with distance.

6.5.2 Nonlinear Wave Propagation

Spikes moving down an axon are but one instance of a *nonlinear propagating wave*. Nonlinear, since in a linear dispersive medium, such as a passive cable, the different Fourier components associated with any particular voltage disturbance will propagate at a different velocity and the disturbance will lose its shape. This is why propagating spikes and the like are frequently referred to by mathematicians as resulting from *nonlinear diffusion*. Other examples include sonic shock waves or the digital pulses in an optical cable.

Scott (1975) argues for a broad classification of such phenomena into (i) those systems for which energy is conserved and which obey a conservation law and (ii) those for which solitary travelling waves imply a balance between the rate of energy release by some nonlinearity and its consumption.

Waves associated with the first type of systems are known as *solitons* and are always based on energy conservation (Scott, Chu and McLaughlin, 1973). Solitons emerge from a balance between the effects of nonlinearity, which tend to draw the wave together, fighting dispersion, which tends to spread the pulse out. This imples that solitons can propagate over a range of speeds. Furthermore, they can propagate through each other without any interference. Solitons have been observed in ocean waves and play a major role in high-speed optical fibers.

Action potentials are an example of the second type of propagating wave, similar to an ordinary burning candle (Scott, 1975). Diffusion of heat down the candle releases wax which burns to supply the heat. If P is the power (in joules per second) necesssary to feed the flame and E the chemical energy stored per unit length of the candle (joules per meter), the nonlinear wave in the form of the flame moves down the candle at a fixed velocity u given by

$$P = uE\,. \tag{6.28}$$

In other words, the velocity is fixed by the properties of the medium and does not depend on the initial conditions. Were we to light flames at both ends of the candle, the flames would move toward each others and annihilate themselves. This is also true if action potentials are initiated at the opposite ends of an axon. When they meet, they run into each others refractory period and destroy each other. Thus, spikes are not solitons.

6.6 Action Potential Propagation in Myelinated Fibers

The successful culmination of the research effort by Hodgkin and Huxley heralded the coming of age of neurobiology. While we will deal in chapter **??** with their methodology as applied in the past decades to the ionic currents found at the cell body of nerve cells, let us here briefly summarize spike propagation in *myelinated* axons (for more details, see Waxman, Kocis, Stys, 1995; Ritchie, 1995; Weiss, 1996).

Axons come in two flavors, those covered by layers of the lipid *myelin* and those that are not. The squid axon is an unmyelinated fiber, common to invertebrates. In vertebrates, many fibers are wrapped dozens or even hundreds of time with myelin, the actual diameter

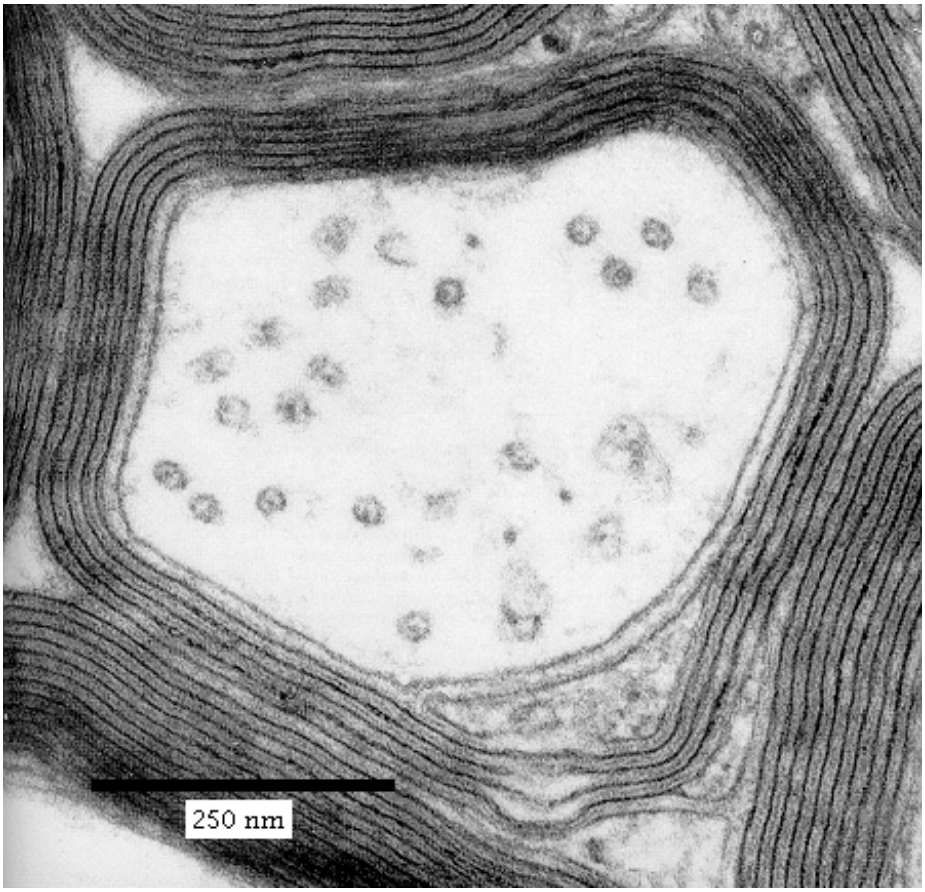

Figure 6.14: MYELINATED AXONS
Electron micrograph of a cross section through portion of the optic fiber in an adult rat. The complete transverse section through a single myelinated axon is shown, in close neighbourhood to other axons.
About four wrappings of myelin insulation are visible. The circular structures inside the axonal cytoplasm are transverse sections through microtubules. From Peters, Palay and Webster (1976).

---

of the axon itself being only 60% or 70% of the total diameter (Fig. 6.14). This insulating material is formed by special supporting cells, called *Schwann* cells in the peripheral nervous system and *oligodendrocytes* in the central nervous system.

A second specialization of myelinated fibers is that the myelin sheet is interrupted at regular intervals along the axon by nodes, named for their discoverer *nodes of Ranvier*. Here, the extracellular space gains direct access to the axonal membrane. Typically, the length of a node is very small (0.1%) compared to the length of the *internodal* segment (Fig. 6.15). In the vertebrate, single myelinated fibers range in diameter from 0.2-20 μm, while unmyelinated fibers range between 0.1-1 μm. In stark contrast, the diameter of unmyelinated invertebrate fibers range from under 1 μm to 1 mm.

In myelinated axons, conduction does not proceed continuously along the cable, but jumps in a discontinuous manner from one node to the next. This *saltatory conduction* (from the Latin *saltus*, to leap) was clearly demonstrated by Huxley and Stämpfli (1949) and Tasaki (1956). What these and similar experiments on frog, rabbit and rat myelinated fibers made clear is that ionic currents are strikingly inhomogeneous distributed across the axonal membrane (Fig. 6.15; FitzHugh, 1962; Frankenhaeuser and Huxley, 1964; Stämpfli and Hille, 1976; Rogart and Ritchie, 1977; Chiu, Ritchie, Rogart and Stagg, 1979; Chiu and Ritchie, 1980). Spike generation essentially only takes places at the small nodes of Ranvier, which are loaded with fast, sodium channels (between 700 and 2000 per μm^2). In mammalian myelinated nerves, the repolarization of the spike is not driven by an large outward potassium current, as in the squid axon[6] but is achieved using a rapid sodium inactivation in combination with a large effective leak conductance. Indeed, action potentials do not show any hyperpolarization (Fig. 6.1B), unlike those in the squid giant axon. The origin of the large, voltage-independent leak might involve an extracellular pathway beneath the myelin that connects the nodal and internodal regions (Barrett and Barrett, 1982; Ritchie, 1995). Potassium channels are present under the myelin sheet along the internodal section, although their functional role is unclear (Waxman and Ritchie, 1985).

The function of the numerous, tightly drawn layers of myelin around the internodal segments is to reduce the huge capacitive load imposed by this very large cable segment, as well as to reduce the amount of longitudinal current that leaks out across the membrane. The effective membrane capacitance of the entire myelin sheath, made up in the case of the frog axon illustrated in Fig. 6.15 out of 250 myelin layers, is $C_m/250$ with C_m the specific capacitance of one layer of myelin (similar to that of the axonal membrane), while the effective resistance is 250 times higher than the R_m of one layer of myelin. Even though the length of the interaxial node is typically 1,000 times larger than the node, its total capacitance has the same order of magnitude (Fig. 6.15). This allows the action potential to rapidly spread from one node to the next, "jumping" across the intervening internodal area and reducing metabolic cost (since less energy must be expended to restore the sodium concentration gradient following action potential generation). There is a safety factor built into the system, since blocking one node via a local anesthetic agent does not prevent blockage of the impulse across the node (Tasaki, 1953). Detailed computer simulations of the appropriately modified Hodgkin-Huxely equations (based on the circuit shown in Fig. 6.15) have confirmed all of this (Frankenhaeuser and Huxley, 1964; Rogart and Ritchie, 1977).

Single axons can extend over one meter or more[7], making conduction velocity of the electrical impulses something that evolution must have tried to minimize at all cost. Measurements (Huxley and Stämpfli, 1949) and computations indicate that the time it takes for the currents at one node to charge up the membrane potential at the next node is limited by the time it takes to charge up the intervening internodal membrane. This is determined by the time constant of the membrane τ, which is independent of the geometry of the axon. In

[6]Pharmacological blockage of potassium channels has no effect on the shape of the action potential in the rabbit fibers (Ritchie, Rang and Pellegrino, 1981).

[7]Think about the spinal nerve axons of an elephant or of the extinct Brontosaurus.

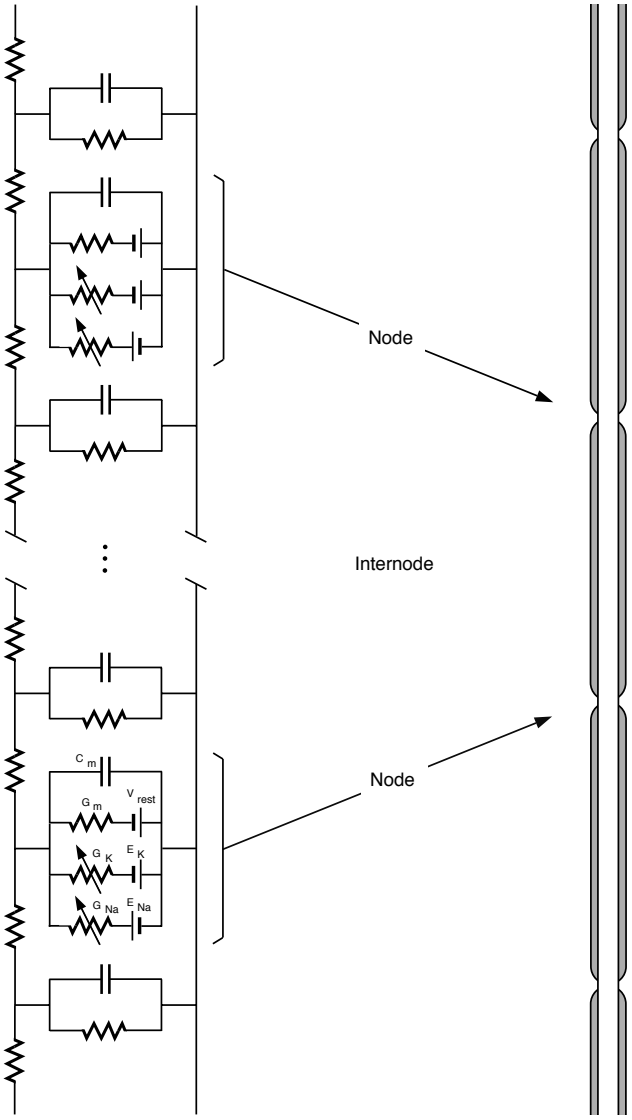

Figure 6.15: Electrical Circuit for a Myelinated Axon

Geometrical and electrical layout of the myelinated axon from the frog sciatic nerve (Frankenhaeuser and Huxley, 1964; Rogart and Ritchie, 1977). The diameter of the axon and its myelin sheath is 15 μm, the diameter of the axon itself 10.5 μm, the difference being made up by 250 wrappings of myelin. The myelin is interrupted every 1.38 mm by a *node of Ranvier* that is 2.5 μm wide. The total distributed capacitance for the internode (2.2 pF) is only slightly larger than the capacitance of the much smaller node (1.6 pF). The same is also true of the distributed resistance. At each node, the spike is re-amplified by a fast sodium current and is repolarized by a potassium current. Little or no potassium current is found at the nodes of Ranvier in mammalian myelinated axons. There, repolarization is accomplished by rapid sodium inactivation in conjunction with a large effective "leak" current.

this time the spike will have moved across the internodal distance, making the propagation velocity proportional to this distance divided by τ. Since anatomically, the internodal distance is linearly related to the diameter of the axon, the velocity of spike propagation will be proportional to the fiber diameter,

$$u \propto d\,, \tag{6.29}$$

rather than the square root dependency found for unmyelinated fibers (eq. 6.27). Rushton (1951) gave this argument a precise form using the principle of *dimensional scaling*. If, he argued, axons had the same specific membrane properties, then in order for points along two axons with different diameters to be in "corresponding states", certain scaling relationships must hold. In particular, space should increase in units of the internodal length and velocity should be roughly proportional to the fiber diameter (for more details, see Weiss, 1996). The latter is actually the case (Fig. 6.16). When comparing the fiber diameter against the propagation velocity for myelinated cat axons, a roughly linear relationship can be observed (Hursh, 1939; Rushton, 1951; Ritchie, 1982). With the exception of a 1.1 μm thick unmyelinated mammalian fiber that propagates action potentials at 2.3 mm/msec (Gasser, 1950), spike velocity in very small fibers has, so far, been difficult to record.

The functional importance of myelinated fibers is clear. They provide a reliable and rapid means of communicating impulses at a much reduced cost compared to unmyelinated fibers (at the same conduction velocity, an myelinated fiber can be up to 50 times smaller than an unmyelinated fiber). This large ($\times$ 2500) factor in packing allows the brain to squeeze more than a million axons into a single nerve that supplies the brain with visual information. The primary cost of this insulation is the added developmental complexity and the possibility that demyelinating diseases, such as *Multiple Sclerosis*, can incapacitate the organism.

6.7 Branching Axons

The all-or-none nature of action potentials has lead to the idea that the axon serves mainly as a reliable transmission line, making a highly secure, one way, point-to-point connection among two processing devices. Furthermore, because of its high propagation velocity, the action potential is thought to arrive almost simultaneously to all of its output sites. Indeed, both properties have been used to infer that spikes propagating parallel fibers in the cerebellum serve to implement a very precise timing circuit (Braitenberg and Atwood, 1958; Braitenberg, 1967).

It will not come as a surprise that the axon-as-a-wire concept is not quite true and needs to be revised. Experimentally, it is know that trains of action potentials show failure at certain regions along the axon, most likely at the branch points. In other words, the train of spikes generated at the soma may have lost some of its members by the time it reaches the presynaptic terminals, with individual spikes "deleted" (Barron and Matthews, 1935; Tauc and Hughes, 1963; Chung, Raymond and Lettvin, 1970; Parnas, 1972; Smith, 1983). For instance, conduction across a branching point in a lobster axon fails at frequencies above 30 Hz (Grossman, Parnas and Spira, 1979a). This conduction block first appears

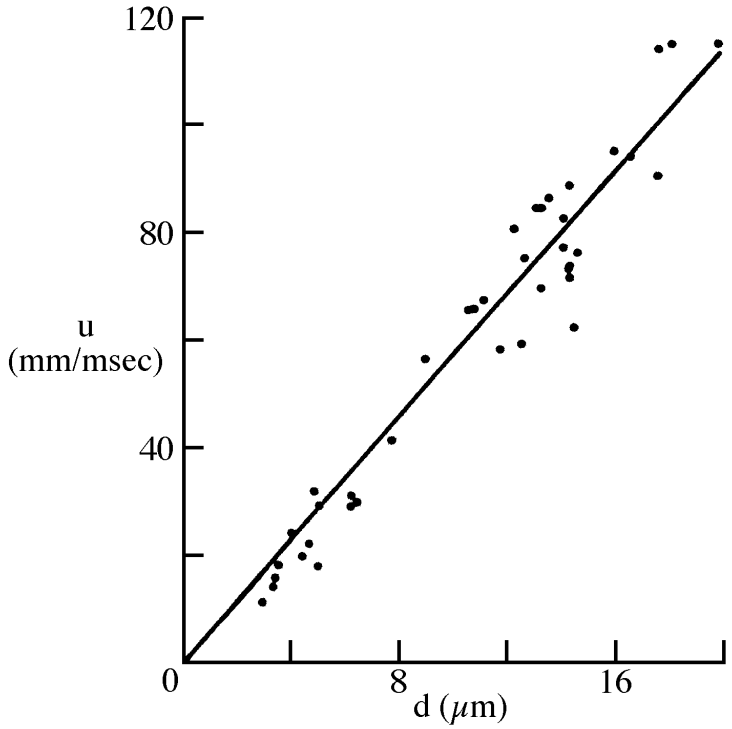

Figure 6.16: DIAMETER AND PROPAGATION VELOCITY
The relationship between the (internal) diameter d of adult cat peripheral myelinated fibers and propagation velocity u of the action potential. The data are shown as dots (Hursh, 1939) and the least square fit as a line. Peripheral myelinated fibers are bigger than 1 μm, while myelinated fibers in the central nervous system can be as thin as 0.2 μm, with an expected velocity in the 1 mm/msec range. From Ritchie (1982).

---

in the thicker daughter branch and only later in the thinner branch, most likely due to a differential buildup of potassium ions (Grossman, Parnas and Spira, 1979b). Physiological evidence indicates that such a switching mechanism might subserve a specific function in the case of the motor axon innervating the muscle used for opening the claw in the crayfish (Bittner, 1968). Depending on the firing frequencies, spikes are routed differentially into two branches of the axon going to separate muscle fibers.

These experimental studies have shown that action potentials may fail to successfully invade the daughter branches of a bifurcating axon. As the theoretical analysis by Goldstein and Rall (1974) pointed out, the single most important parameter upon which propagation past the bifurcation depends is its associated geometric ratio

$$GR = \frac{d_{daughter,1}^{3/2} + d_{daughter,2}^{3/2}}{d_{parent}^{3/2}}, \tag{6.30}$$

where the d's are the fiber diameters and it is assumed that the specific membrane properties

are constant in all three branches. This should remind us, of course, of the analysis of the branching passive cables (sections 3.1 and 3.2 and eq. 3.15) and, indeed, the reasoning is identical. GR equals the ratio of the input impedances if all cables are semi-infinite.

Goldstein and Rall's (1974) and subsequent analytical and modeling investigations (Khodorov and Timin, 1975; Parnas and Segev, 1979; Moore, Stockbridge and Westerfield, 1983; Lüscher and Shiner, 1990a,b; Manor, Koch and Segev, 1991) established the following principles. For $GR = 1$, *impedances match* perfectly and the spike propagates without any perturbation past the branch point (indeed, electrically speaking, for $GR = 1$ the branching configuration can be reduced to a single *equivalent cable*, albeit an active one; see section 3.2). If $GR < 1$, the action potential behaves as if the axon tapers and it will slightly speed up. The far more common situation is $GR > 1$, *i.e.* the combined electrical load of the daughters exceeds the load of the main branch. As long as GR is approximately < 10, propagation past the branch point is assured, although with some delay (that can be substantial for large values of GR). If $GR > 10$, propagation into both branches fails simultaneously, since the electrical load of the daughters has increased beyond the capacity of the electrical current from the parent branch to initiate a spike in the daughter branches. Parnas and Segev (1979) emphasize that for each constant geometric ratio, changes in the diameter ratio between the daughter branches never yields differential conduction into one of the daughters if the specific membrane properties are identical in both. This implies that the experimentally observed differential conduction (Bittner, 1968; Grossman, Parnas and Spira, 1979a) must be due to other factors, such as a run-down in the ionic concentration across the membrane or saturation of the ionic pumps that are sensitive to the ratio of area-to-volume (and would thus be expected to occur earlier in larger fibers). Note that all of these modeling studies have assumed unmyelinated fibers and that axonal branch points appear to be devoid of myelin.

Up to ten to twelve bifurcations (see the heavily branched axonal terminal arbor in Fig. 3.1M) can occur before the action potential reaches its presynaptic terminal where it initiates vesicular release. The delay at branch points with $GR > 1$, in conjunction with other geometrical inhomogeneities, such as the short swellings at sites of synaptic terminals called *varicosities*, might add up to a considerable number, leading to a substantial broadening of spike arrival times at their postsynaptic targets.

The degree of temporal dispersion was simulated in the case of an axon from the somatosensory cortex of the cat (Manor, Koch and Segev, 1991). Since it is almost entirely confined to cortical gray matter, it was taken to be unmyelinated (Fig. 6.17). In the absence of better data, Hodgkin-Huxley dynamics (at 20° C) were assumed. About 1,000 boutons were added to the axon and the propagation time between spike initiation just beyond the cell body and these boutons was histogrammed (Fig. 6.17). The first peak (with a mean of 3.8± 0.5 msec) is contributed from terminals along the branches in cortical areas 3a and 3b (see the inset in Fig. 6.17) and the more delayed one from those in area 4 (mean of 5.8± 0.4 msec). Of the total delay, about 22-33% of the delay is due to the branch points and geometrical inhomogeneities; the majority is simple propagation delay. Manor *et al.*, (1991) conclude that temporal dispersion in the axonal tree will be minor, on the order of 0.5-1 msec.

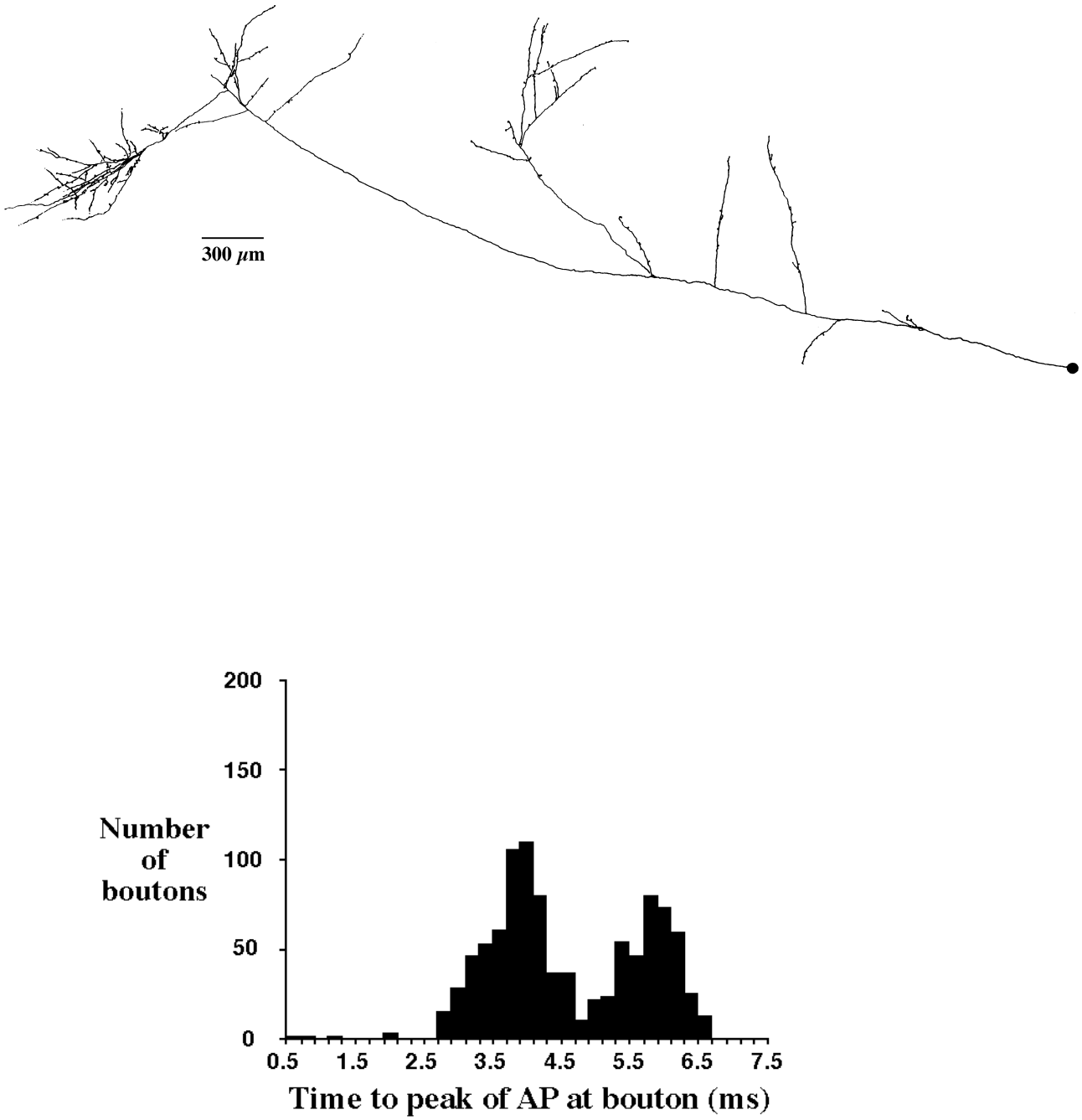

Figure 6.17: Propagation Delays along a Branching Axon

What delays do action potential incur as they propagate through a highly branching axonal tree? This was simulated in the case of an HRP labeled axon originated in layer 5 of the somatosensory cortex of the adult cat. The drawing of the axon is from Schwark and Jones, (1989). Histogram of the delay incurred between action potential initiation just beyond the cell body and the 977 terminals distributed in the terminal branches of the axon is shown at the bottom. The two humps correspond to synapses from the proximal and the distal part of the axonal tree. Over the 3.5 mm of the tree, the total delay is 6.5 msec and temporal dispersion is minimal. From Manor *et al.*, (1991).

Let us conclude with one observation. Computer simulations of branching axons (Segev, I., O'Donnell, P. and Koch, C., unpublished manuscript) have shown that a strategically located inhibitory synapse of the shunting type onto one branch of the axon, following the on-the-path theorem (section 5.1.3), can selectively veto an action potential from invading this branch while not affecting spike invasion into the second branch. This would allow for very fast synaptic switching or *routing* of information in an axonal tree (similar to a telephone network). While inhibitory synapses can be found directly at the axon initial segment (Kosaka, 1983; Soriano and Frotscher, 1989), no synapses, whether excitatory or inhibitory, have been observed on or around axonal branching points. It is anybody's guess why the nervous system did not avail itself of this opportunity to precisely (in space and time) filter or gate action potentials.

6.8 Recapitulation

The Hodgkin and Huxley 1952 model of action potential generation and propagation is the single most successful, quantitative model in neuroscience. At its heart is the depiction of the time- and voltage-dependent sodium and potassium conductances G_{Na} and G_K in terms of a number of gating particles. The state of G_{Na} is governed by three activation particles m and one inactivating particle h, while the fate of the potassium conductance is regulated by four activating particles n. The dynamics of these particles are governed by first-order differential equations with two voltage-dependent terms, the steady-state activation (or inactivation) and the time constant. The key feature of activating particles is that their amplitude increases with increasing depolarization, while the converse in true for inactivating particles. For rapid input to a patch of squid axonal membrane, spike initiation is exceeded whenever the net inward current becomes negative, that is when a particular voltage threshold V_{th} is exceeded.

Inclusion of the cable term leads to a four-dimensional system of coupled, nonlinear differential equations with a wave solution that propagates at a constant velocity down the axon. This wave, the action potential, is due to the balance between dispersion and restoration caused by the voltage-dependent membrane. When injecting sustained currents into the axon, the equations predict two important aspects of the squid axon: the abrupt onset of sustained firing with a high spiking frequency and the very limited bandwidth of the firing frequency.

Hodgkin-Huxley's formalism continues to be used in all but a handful of today's quantitative models of nerve cell excitability, constituting a remarkable testimony to the brilliance of these researchers. It should be remembered that their model was formulated at a time when the existence of ionic channels, the binary, microscopic and stochastic elements underlying the continuous, macroscopic and deterministic ionic currents, was not known.

Wrapping axons in insulating material, such as the many layers of myelin observed in myelinated fibers that are found in all vertebrates, leads to a dramatic speedup over unmyelinated fibers. Conversely, at the same spike propagation speed, myelinated fibers can be up to 50 times thinner than unmyelinated fibers. In mammals, axons above 1 μm are usually myelinated, with speeds in the 5 mm per millisecond range, and rarely exceed 20 μm. When

axons reach their target zone, they branch profusely, enabeling them to make thousands of contacts on postsynaptic processes. As train of spikes attempt to propagate past these points, they can be slowed down, depending on the exact geometry of the junction. In the more extreme cases, individual spikes can fail to propagate past branch points.

We conclude that pulses can communicate along axons reliably, rapidly (at speed between one and one hundred millimeters per millisecond) and with little temporal dispersion. The main exception to this appears to be propagation of trains of spikes past branching points. Here, due to a variety of phenomena, conduction block can occur that will differentially route information into one of the daughter branches or prevent conduction alltogether.